Role of HPC in Molecular Simulation

In

The Workshop on

High Performance Computing and its Multidisciplinary Applications

August 26, 2022

Dr. Amit Kumar Paul

Department of Chemistry,

National Institute of Technology Meghalaya

Advantages

- Get to know atomistic details of any chemical phenomena
- Information at extreme situations, at molecular level or environmental conditions, where experiments are impossible, can be obtained
- For a chemical reaction, experiment may see one product, but simulation results can show all possible pathways
- Based on an experimental observation, predictions can be made which can guide an experimentalist
- In most of the cases, experimental observations are explained from MD simulations

Disadvantages

- Accurate Potential energy is needed. A wrong PE can predict wrong result
- Initial conditions should be properly incorporated
- Authenticity should be cross checked, preferably, experimentally.

Molecular Simulation (Molecular Dynamics)

Quantum Dynamics

Wavefunction dynamics or
Schrödinger dynamics

Classical Dynamics

Newtonian Dynamics

Lagrangian Dynamics

Hamiltonian Dynamics

Quantum Dynamics

- Schrödinger equation is solved

$$i\hbar \frac{\partial \psi(t)}{\partial t} = \hat{H}\psi(t)$$

- Ψ is a state function, $\hat{H}$ is Hamiltonian which is the sum of kinetic and potential energy operators.
- Potential energy changes from system to system and for bigger molecular systems it becomes so complex that makes it difficult to solve Schrödinger equation.

Quantum Dynamics

- Hamiltonian:

$$\hat{H} = \sum_{n=1}^{N} \hat{T}_n + \hat{V}$$

$$= \sum_{n=1}^{N} \frac{\hat{\mathbf{p}}_n \cdot \hat{\mathbf{p}}_n}{2m_n} + V(\mathbf{r}_1, \mathbf{r}_2, \ldots, \mathbf{r}_N, t)$$

$$= -\frac{\hbar^2}{2} \sum_{n=1}^{N} \frac{1}{m_n} \nabla_n^2 + V(\mathbf{r}_1, \mathbf{r}_2, \ldots, \mathbf{r}_N, t)$$

- Initial wavefunction:

$$\psi^{adia}(x, t_0) = \left(\frac{1}{2\pi\Delta x^2} \right)^{1/4} \exp\left(-\frac{(x - x_0)^2}{4\Delta x^2} \right)$$

Outcome of QD

Autocorrelation function

$$C(t) = \langle \psi(t) | \psi(0) \rangle$$

$$C(t) = \langle \psi(t) | \psi(0) \rangle = \left\langle \psi^* \left(\frac{t}{2} \right) | \psi \left(\frac{t}{2} \right) \right\rangle$$

Fourier Transformation

$$I(\omega) \propto \int_{-\infty}^{\infty} C(t) \exp(i\omega t) dt$$

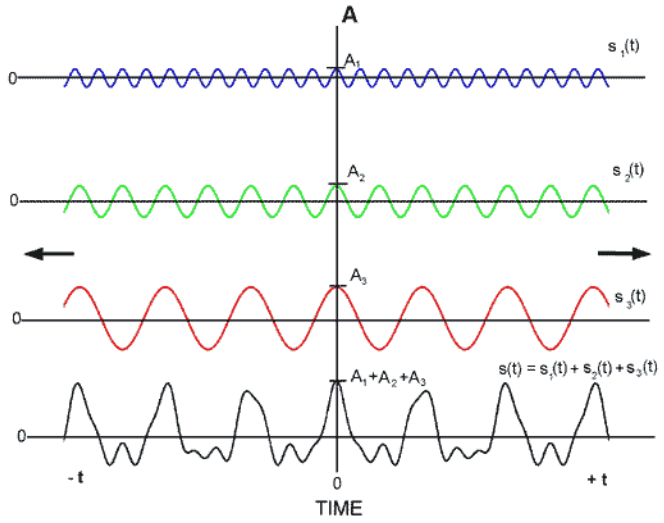

FT

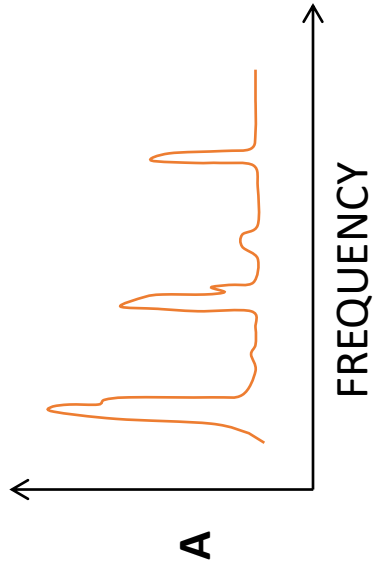

Photoabsorption Spectra of Na_3

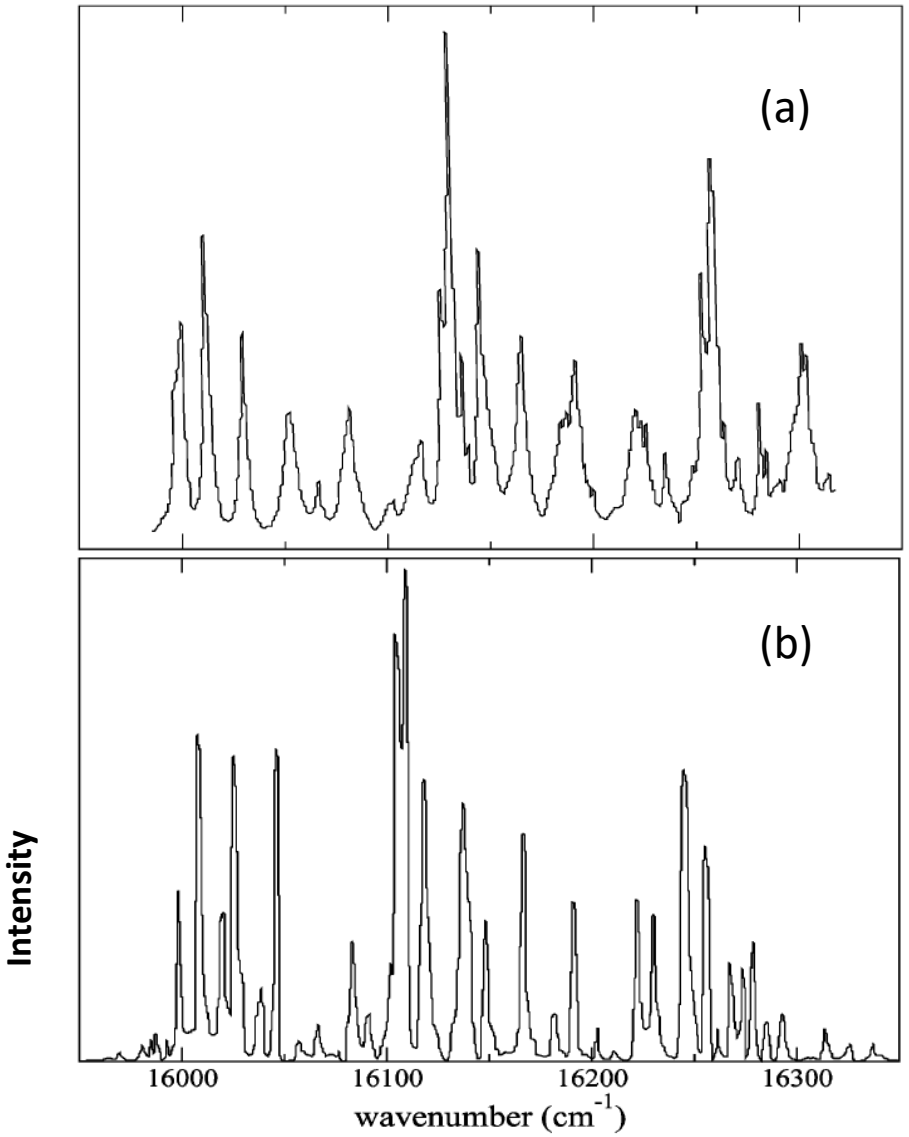

a. Experimental Spectra* (RTPI) by *Wolfgang Ernst*, Graz, Austria

b. Theoretical spectra

* W. E. Ernst and O. Golonzka, *Phys. Scr.* **T112**, 27 (2004).

Classical Dynamics (Hamiltonian Dynamics)

- Propagates position and momentum by solving Hamilton's equations of motion simultaneously

$$\frac{\partial q_i}{\partial t} = \frac{\partial H}{\partial p_i}; \frac{\partial p_i}{\partial t} = -\frac{\partial H}{\partial q_i}$$

$$H = T + V$$

$$T = \sum_{i=1}^{N} (P_{x_i}^2 + P_{y_i}^2 + P_{z_i}^2) / 2m_i$$

- Choosing initial p_i's and q_i's for each atom in a molecule: Sampling

Sampling

- Various methods can be considered for choosing initial pi's and qi's depending on the experimental conditions, namely, temperature, energy, excitation, etc.
- For Temperature sampling Boltzmann distribution mainly considered

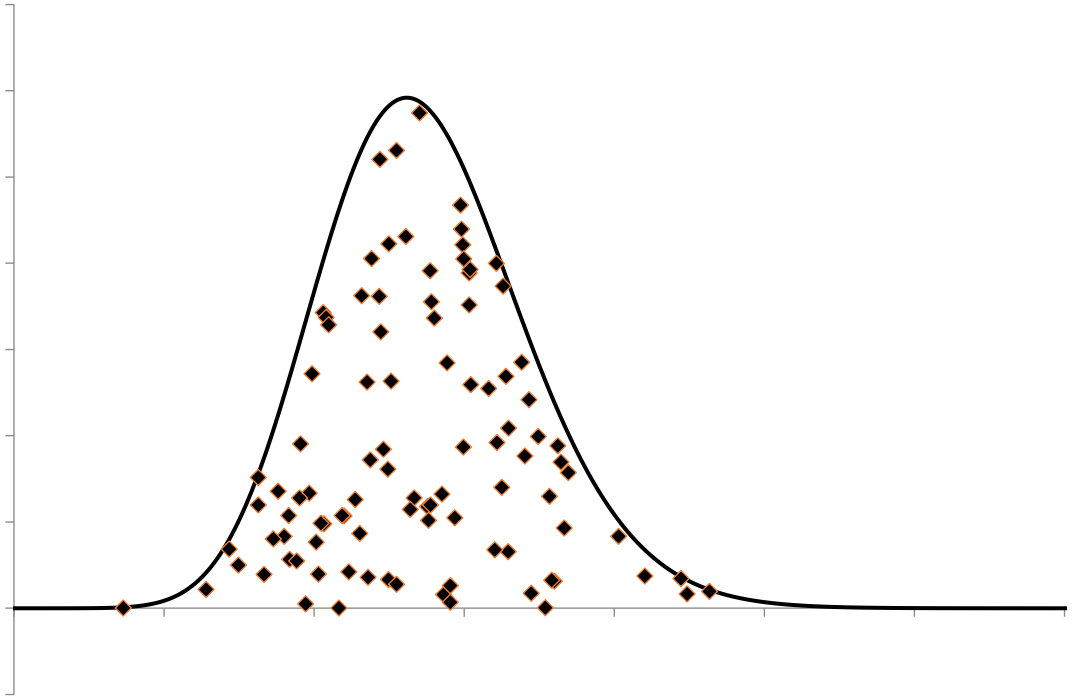

Energy Sampling

- Classical Microcanonical:

$$E_i = \left[E_v^0 - \sum_j^{i-1} E_j \right] \left[1 - R_i^{1/(n-i)} \right]$$

- Quantum Sampling:

$$P(n_i) = \exp(-n_i h\nu_i / k_b T_{\text{vib}})[1 - \exp(h\nu_i / k_b T_{\text{vib}})]$$

Flow Chart

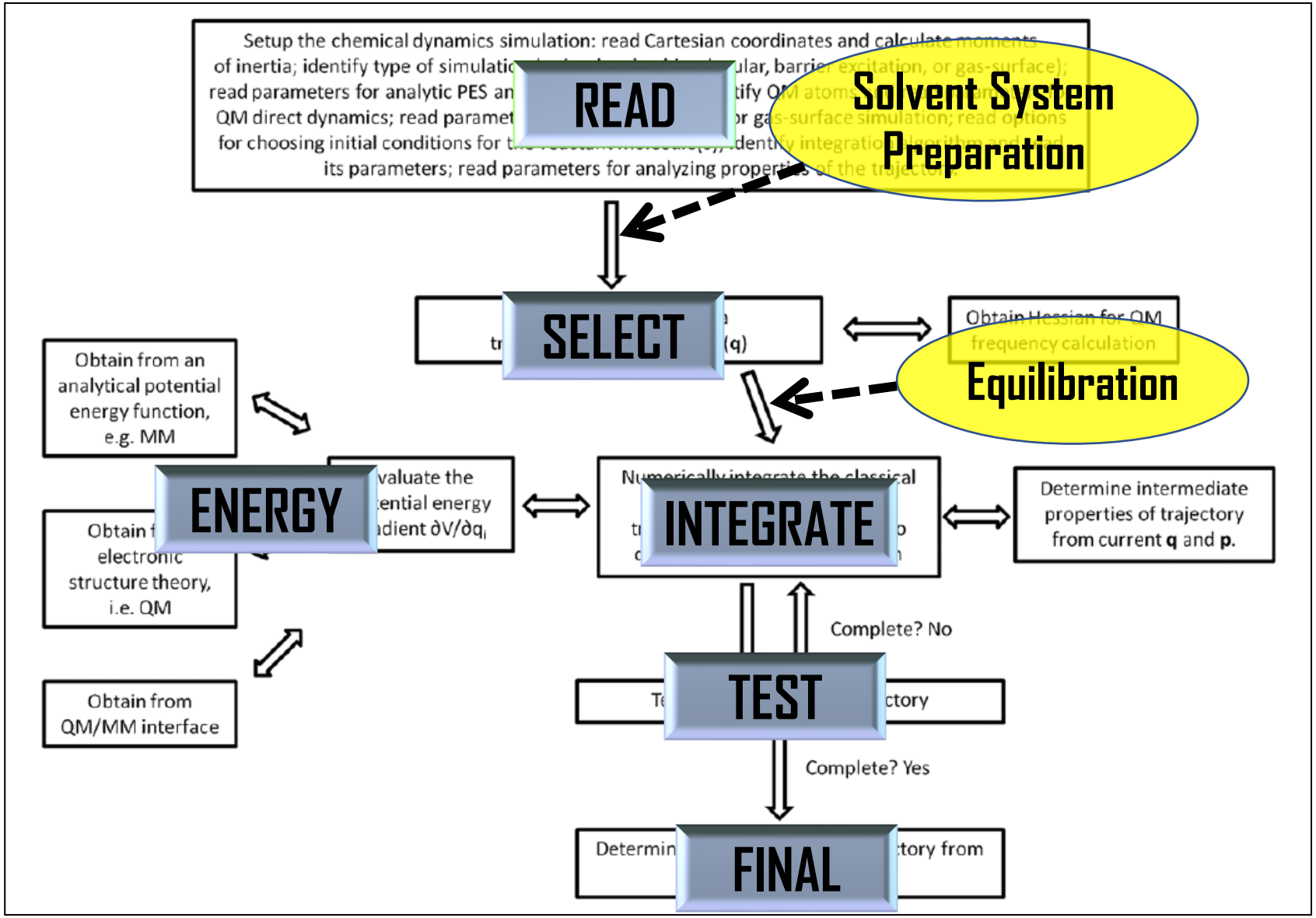

- U. Lourderaj et al, *Computer Physics Communication*, 185, 1074 (2014)
- A. K. Paul et al. J. Chem. Phys. 140, 194103 (2014)

Applications

- Unimolecular Dissociation Dynamics of aromatic complexes

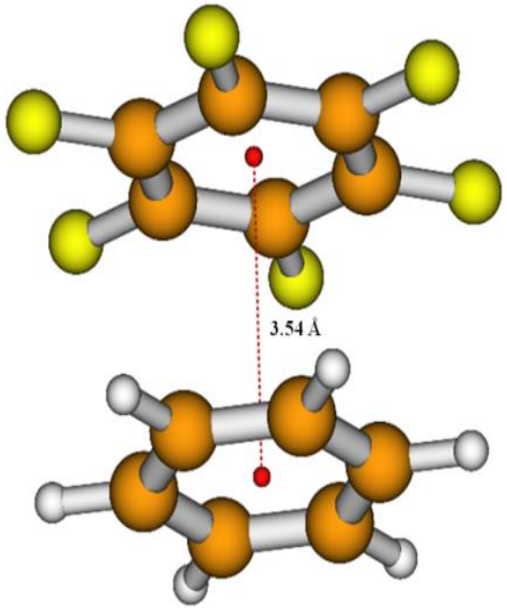

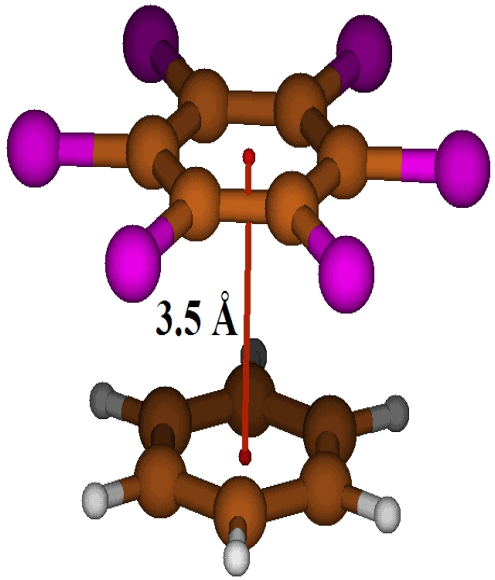

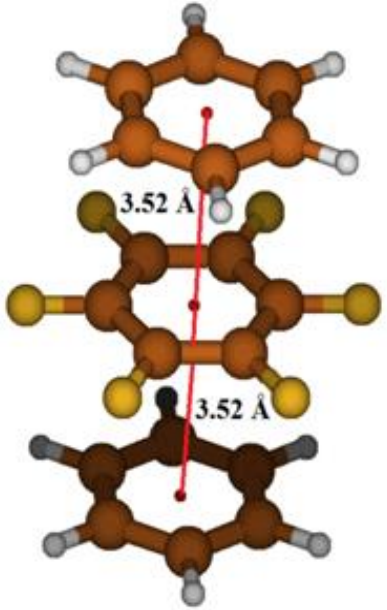

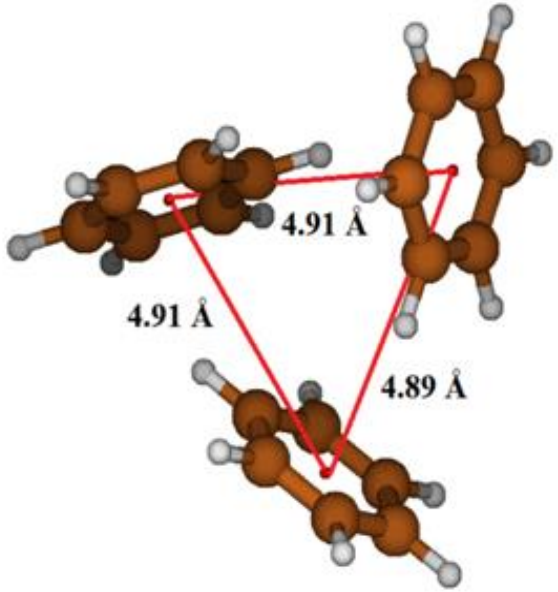

Motive

- Aromatic complexes are of very low binding energies, yet stable at very high temperatures. Why?
- Significant difference between intramolecular and intermolecular frequency values
- IVR issue??

Simulation Initial Conditions

- The complex excitation temperature range of 1000 - 2000 K is considered
- Quantum vibrational energies equivalent to these temperatures are sampled

$$E_{vib} = N \sum_{i=1}^{s} \left(\frac{h\nu_i}{2} + \frac{h\nu_i}{e^{\frac{h\nu_i}{k_B T}} - 1} \right)$$

T (K)	Bz_2	Bz-HFB	Bz-HCB	Bz-trimer	Bz-HFB-Bz
700	156.1	-	-	-	-
800	164.3	-	-	-	-
900	173.1	-	-	-	-
1000	182.4	164.6	163.1	276.8	260.8
1200	202.2	186.4	185.1	307.9	293.7
1500	234.3	220.8	219.7	358.0	346.0
1800	-	256.5	255.6	411.0	400.7
2000	-	280.9	280.1	447.4	438.0

- A quasiclassical microcanonical normal mode sampling is considered to sample those energies to the vibrational modes
- Rotational energies are sampled from a Boltzmann distribution at the corresponding temperature
- 1000 trajectories are integrated up to 30 ps at each temperature.

Results & Discussion: Bz-dimer

Direct Dissociating Trajectories

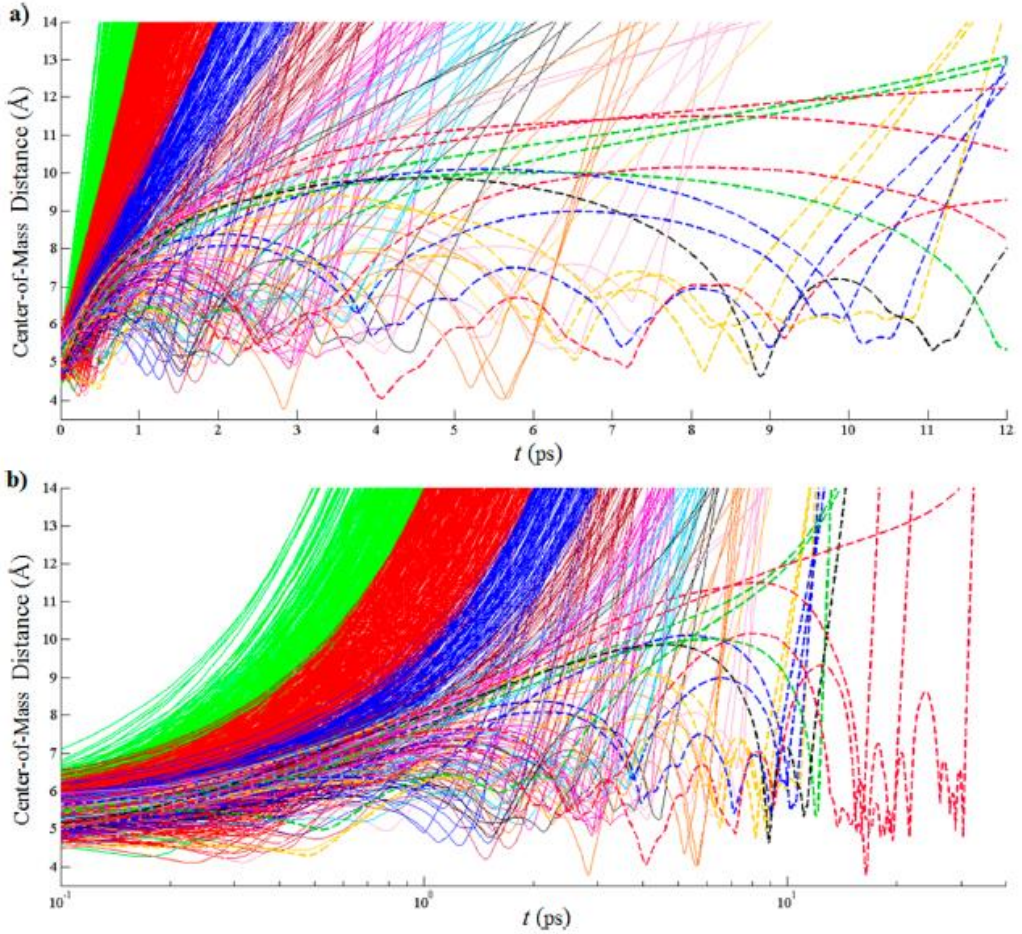

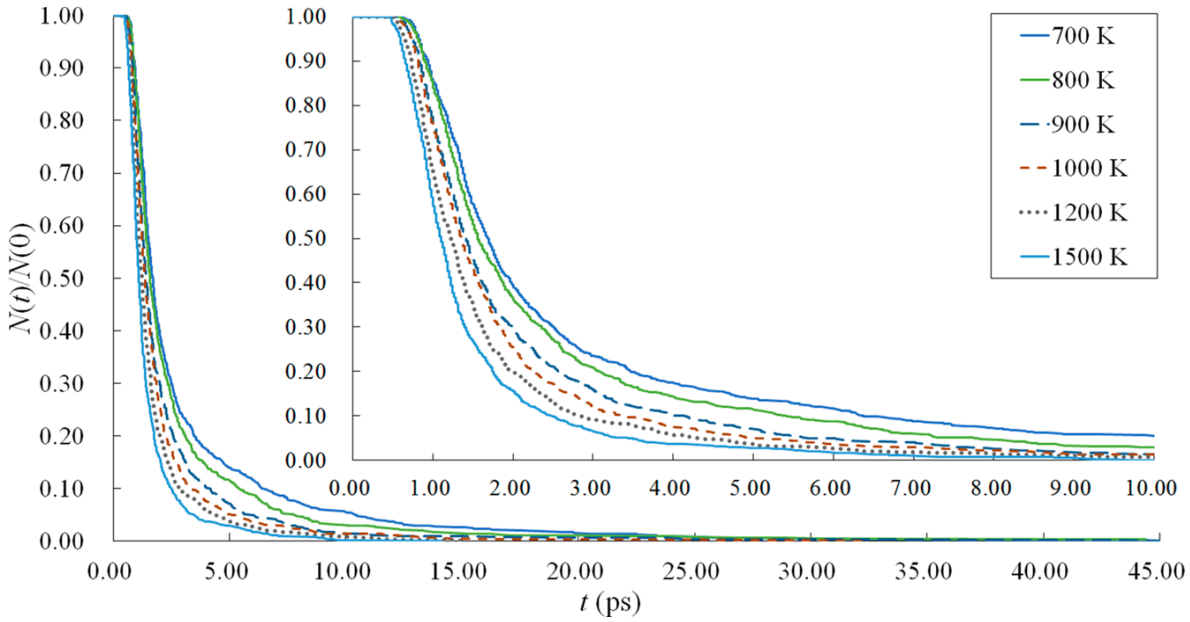

$$\frac{N(t-t_0)}{N(t_0)} = f_1 \exp\left(-k_1(t-t_0)\right) + f_2 \exp\left(-k_2(t-t_0)\right)$$

Ma et al. J. Phys. Chem A, 119, 6631 (2015)

Results & Discussion: Bz-HFB
Fitting Parameters & Microcanonical Rate Constants

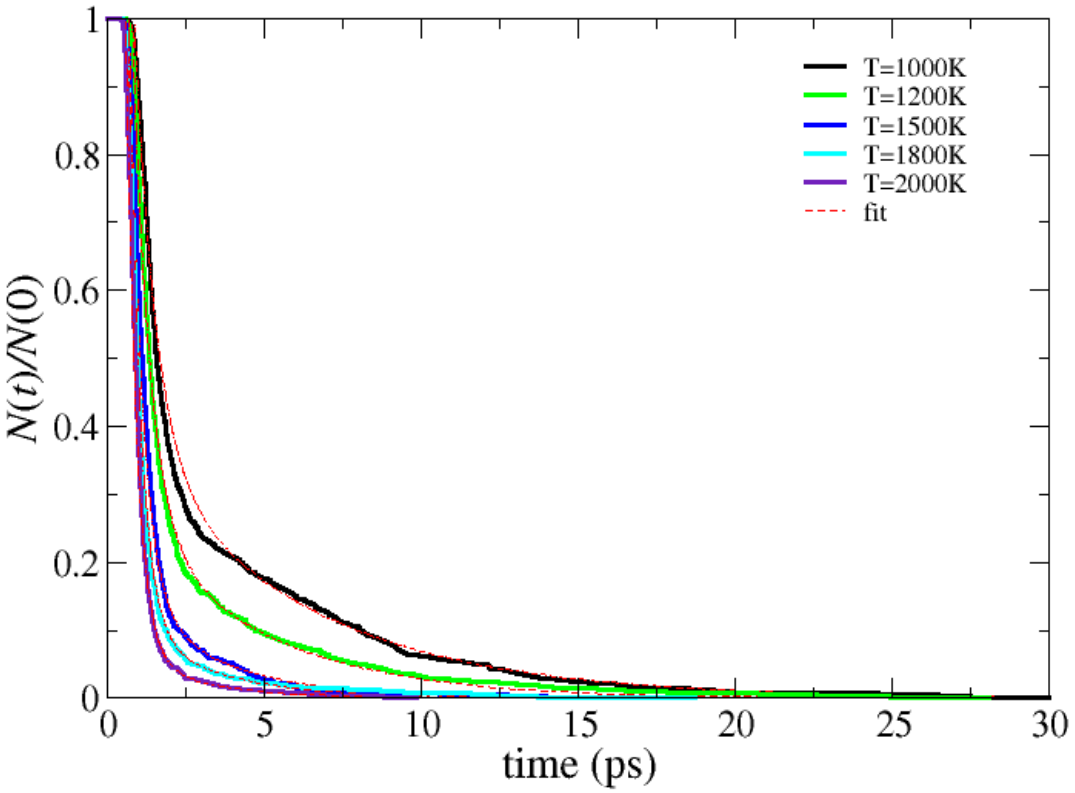

T (K)	f_1	f_2	k_1 (ps^{-1})	k_2 (ps^{-1})	$k(t_0)$ (ps^{-1})
1000	0.64	0.36	1.5	0.18	1.02
1200	0.74	0.26	1.8	0.24	1.43
1500	0.85	0.15	2.4	0.35	2.09
1800	0.89	0.11	2.7	0.38	2.44
2000	0.94	0.06	3.1	0.46	2.94

Arrhenius Parameters: $\mathbf{E_a = 5.0\ kcal/mol}$, pre-exponential factor $\mathbf{(A) = 10.91 \times 10^{12}\ s^{-1}}$

(For reference, Binding energy 5.93 kcal/mol)

H. Mahanta, et al, *J. Phys. Chem. A* **2019**, *123*, 2517-2526.

A Weak Coupling between Intramolecular & Intermolecular Vibrational Modes

trajectory	dissociation time[a] (ps)	E_{inter}[b] (kcal/mol)	E_{intra} (kcal/mol)
a	0.959	18.31	202.6
b	9.181	6.026	214.6
c	0.609	22.29	198.7
d	14.90	6.051	214.7
e	1.938	8.136	213.0
f	5.079	4.532	216.4
g	0.631	15.92	204.9
h	8.498	6.017	214.6

H. Mahanta, et al, *J. Phys. Chem. A* **2019**, *123*, 2517-2526.

Non-Random Excitation of the Complex

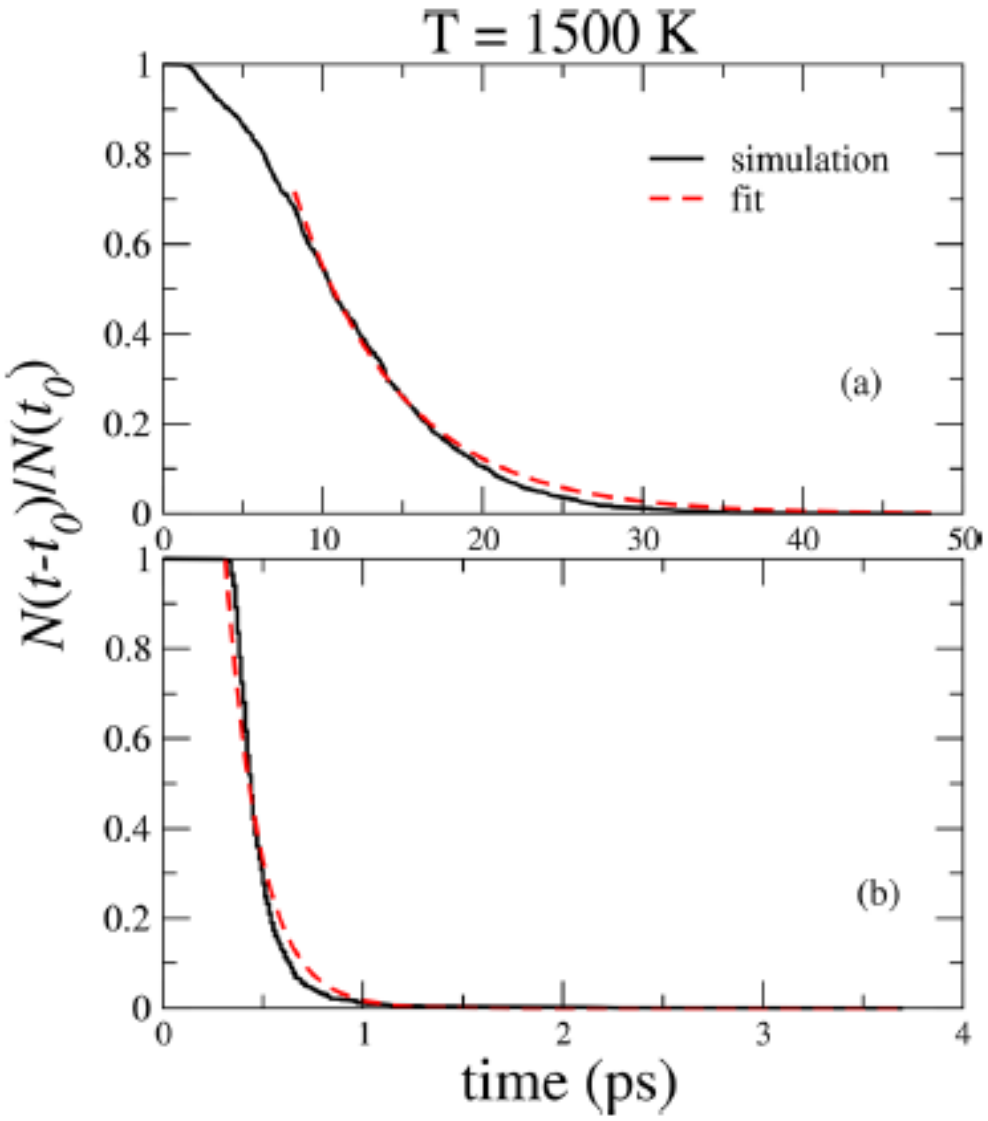

Exponential
$k_{intra} = 0.15\ ps^{-1}$
$k_{inter} = 5.9\ ps^{-1}$

$$P(E) = \int_{E_0}^{\infty} \frac{E^{s-1} e^{-E/k_B T}}{(s-1)!(k_B T)^s}\, dE$$

f_1 = probability that the 6 inter-fragment modes gets energy equal or more than the average vibrational energy at 1500 K (~18 kcal/mol) = 0.44, rate constant = 5.9 ps^{-1}

f_2=1 - f_1 = 0.54, rate constant = 0.15 ps^{-1}

$k(t_0) = f_1 k_1 + f_2 k_2 = 2.68\ ps^{-1}$

From fit at 1500 K, $k(t_0) = 2.09\ ps^{-1}$

The Coupling Improves in Bz-HFB

	initial energy[a]		$k(t_0,E)$ (ps^{-1})	
T (K)	Bz_2	Bz–HFB	Bz_2	Bz–HFB
700	156.1		0.56	
800	164.3		0.69	
900	173.1		0.80	
1000	182.4	164.6	0.88	1.02
1200	202.2	186.4	1.02	1.43
1500	234.3	220.8	1.24	2.09
1800		256.5		2.44
2000		280.9		2.94

[a]The energies are in kcal/mol. Bz_2 dissociation was not performed at 1800 and 2000 K and Bz–HFB at 700, 800, and 900 K.

Binding Energy for Bz-dimer is 2.32 kcal/mol and for Bz-HFB, it is 5.93 kcal/mol. ZPE of intermolecular modes of Bz-dimer is 0.26 kcal/mol and for Bz-HFB is 0.31 kcal/mol

Also, IVR time for Bz-dimer is 20.7 ps and for Bz-HFB is 6.67 ps

H. Mahanta, et al, *J. Phys. Chem. A* **2019**, *123*, 2517-2526.

Possible Reason

Better IVR dynamics, particularly between intermolecular and intramolecular modes

A few vibrational frequencies

Bz-dimer (cm^{-1})	Bz-HFB (cm^{-1})
6.4	1.7
7.7	19
24	19
37	57
41	57
65	68
399.0	126.4
399.0	171.8
612.8	204.3

H. Mahanta, et al, *J. Phys. Chem. A* **2019**, *123*, 2517-2526.

Bz-HCB

Bz-dimer (cm^{-1})	Bz-HFB (cm^{-1})	Bz-HCB (cm^{-1})
6.4	1.7	7
7.7	19	22
24	19	22
37	57	68
41	57	68
65	68	71
399.0	126.4	77
399.0	126.4	77
612.8	171.8	104

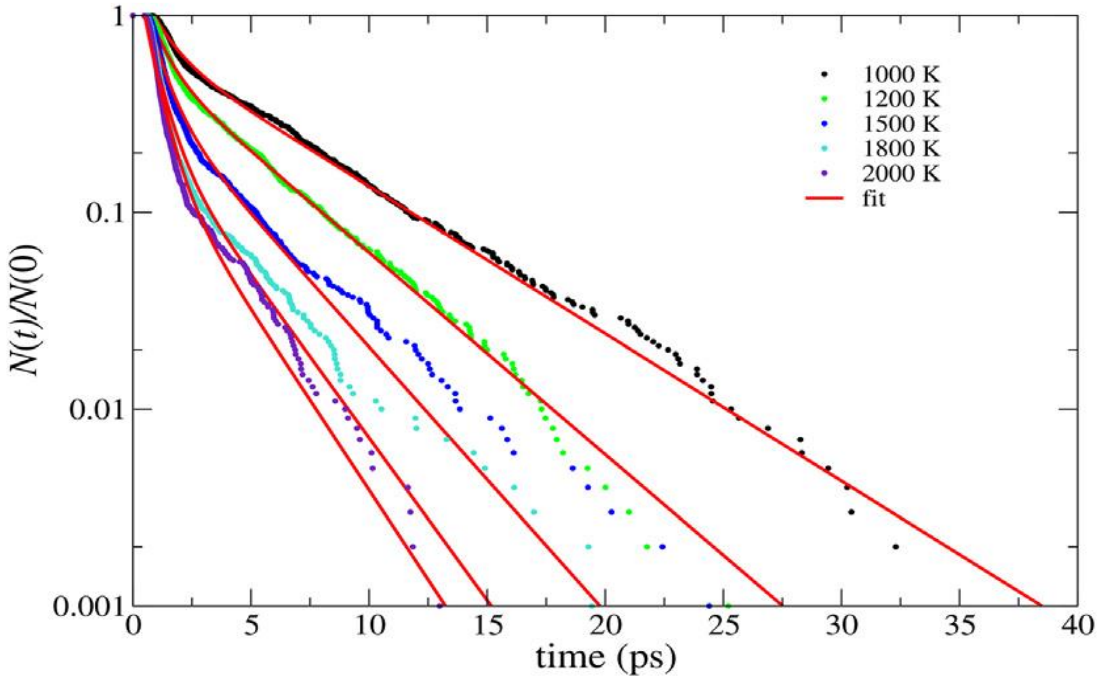

T(K)	E (kcal/mol)	f_1	f_2	k_1 (ps^{-1})	k_2 (ps^{-1})	$k(t_0,E)$ (ps^{-1})[b]
1000	163.1	0.35	0.65	1.06	0.172	0.483
1200	185.1	0.44	0.56	1.30	0.236	0.704
1500	219.7	0.62	0.38	1.40	0.310	0.986
1800	255.6	0.74	0.26	1.60	0.380	1.283
2000	280.1	0.79	0.21	1.65	0.420	1.392

Arrhenius Parameters: **E_a = 5.56 kcal/mol**, pre-exponential factor **(A) = 6.23 x 10^{12} s^{-1}**

(For reference, Binding energy 9.14 kcal/mol)

H. Mahanta, et al. Int. J. Mass. Spect. **2020**, 456, 116392.

Bz-HCB vs Bz-HFB

However, the comparison is just the opposite than expected!!

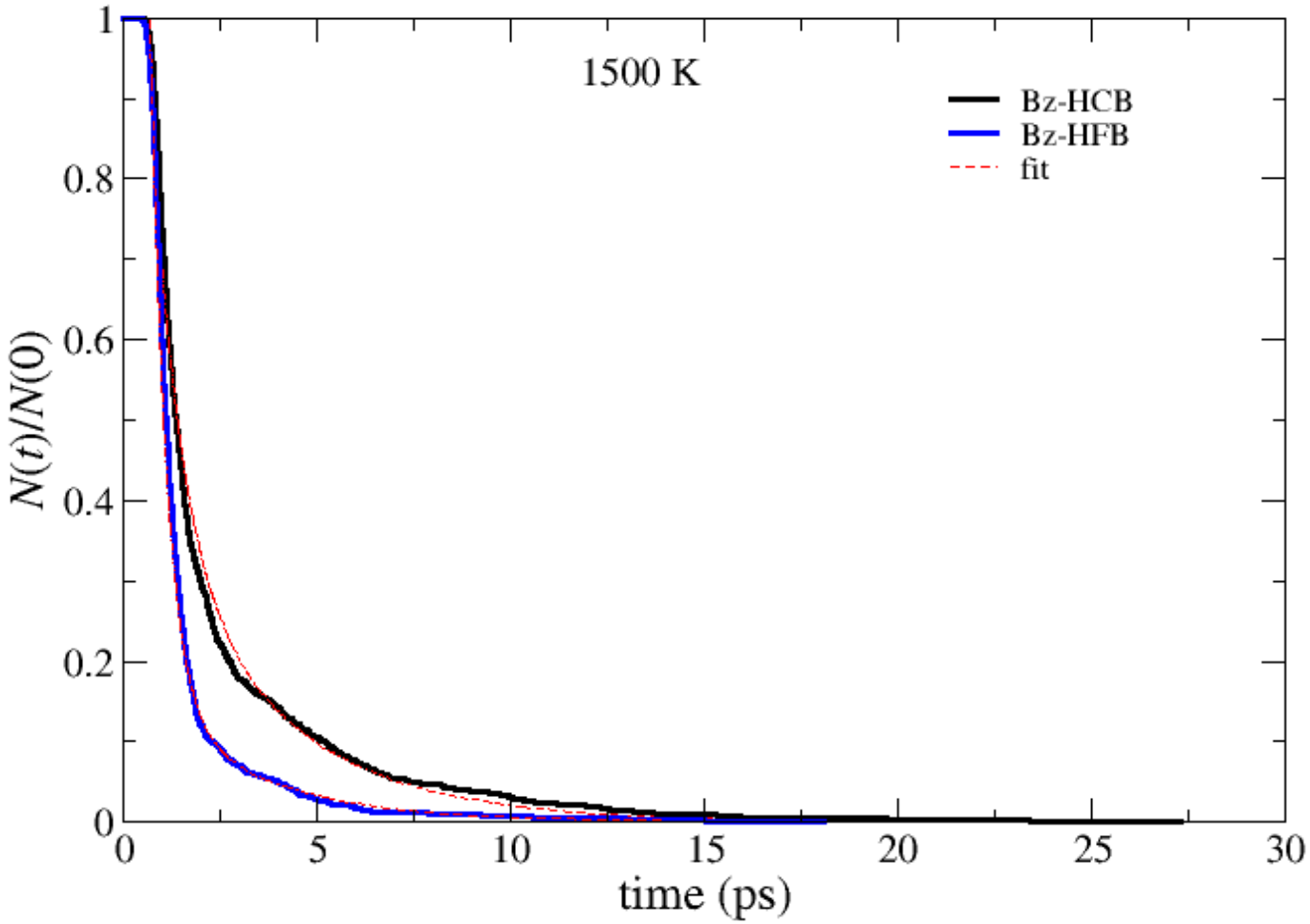

H. Mahanta, et al, *J. Phys. Chem. A* **2021**, *125*, 5870.

Bz-HCB vs Bz-HFB

Frequency group	Mode (υ)	Initial Energy	
		Bz-HFB	Bz-HCB
group 1	υ_1- υ_6	113.4	108.8
group 2	υ_7- υ_{16}	122.4	118.8
group 3	υ_{17}- υ_{26}	119.1	115.5
group 4	υ_{27}- υ_{36}	115.8	111.9
group 5	υ_{37}- υ_{46}	112.9	108.7
group 6	υ_{47}- υ_{56}	109.0	104.9
group 7	υ_{57}- υ_{66}	103.3	98.8
group 8	υ_7- υ_{66}	203.2	202.2

H. Mahanta, et al, *J. Phys. Chem. A* **2021**, *125*, 5870.

Bz-HCB vs Bz-HFB

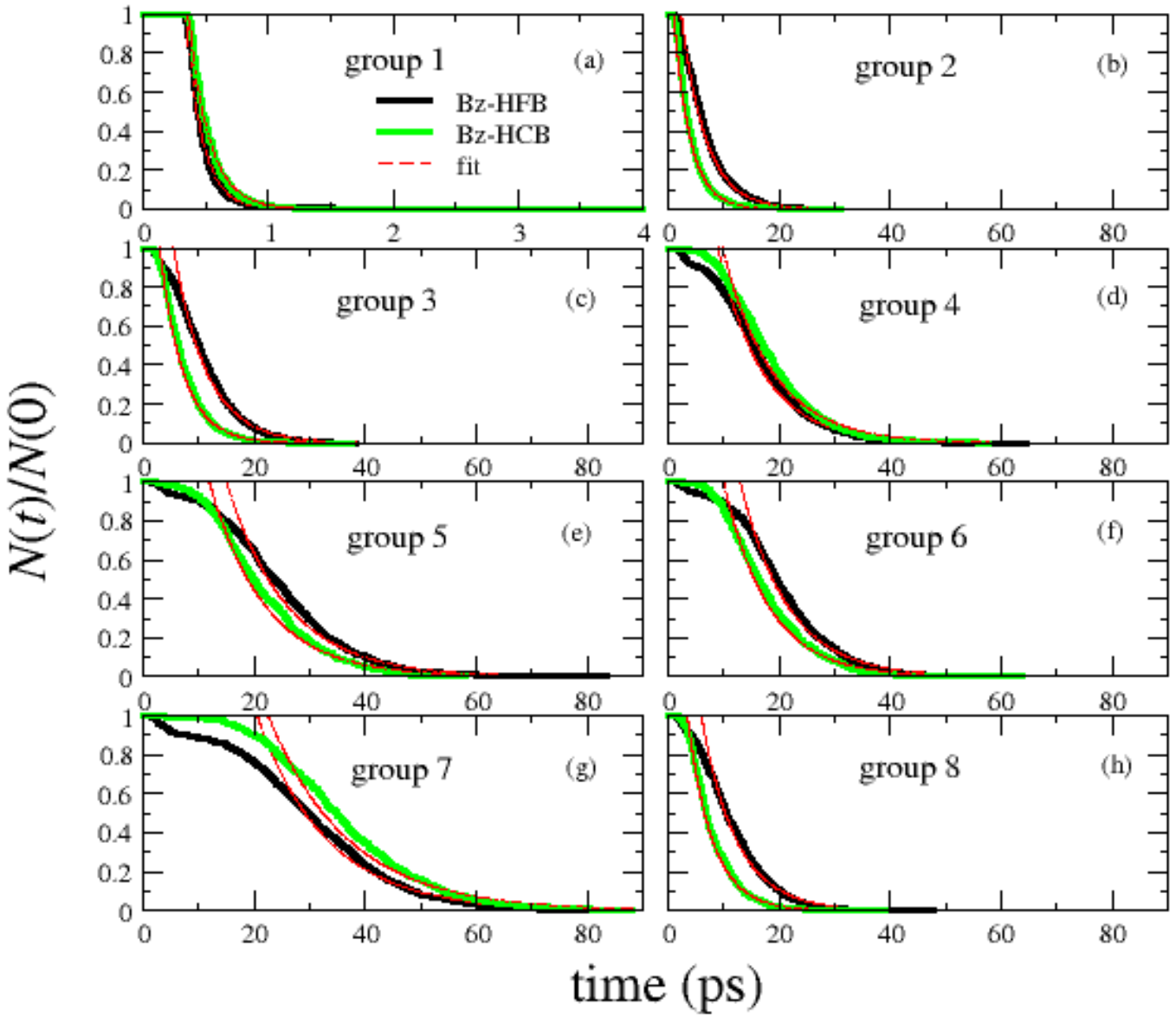

Frequency group excitation	Bz-HCB	Bz-HFB
	$k(t_0)^a$	$k(t_0)^a$
group 1	5.800	5.900
group 2	0.340	0.230
group 3	0.240	0.170
group 4	0.112	0.125
group 5	0.100	0.092
group 6	0.125	0.118
group 7	0.07	0.08
group 8	0.225	0.15

H. Mahanta, et al, *J. Phys. Chem. A* **2021**, *125*, 5870.

Inter-Bz-HCB + a Few Intra-Bz-HCB Vibrational Modes Excitation

Simulations	Mode (υ)	Initial Energy	$k(t_0)$ (ps-1)
1	υ_1- υ_6 + υ_{10}- υ_{12}	117.0	4.2
2	υ_1-υ_6 + υ_{16}-υ_{18}	116.5	4.0
3	υ_1- υ_6 + υ_{26}-υ_{27}	113.2	4.1
4	υ_1- υ_6 + $\upsilon_{28,}$ $\upsilon_{29,}\upsilon_{31}$	115.2	4.1
5	υ_1- υ_6 + υ_{34}- υ_{36}	114.5	4.1
6	υ_1- υ_6 + υ_{37}-υ_{38}	112.4	4.1
7	υ_1- υ_6 + υ_{45}-υ_{47}	113.7	3.4
8	υ_1-υ_6 + υ_{59}-υ_{60}	111.0	4.8
9	υ_1- υ_6 + υ_{63}-υ_{65}	110.3	3.7

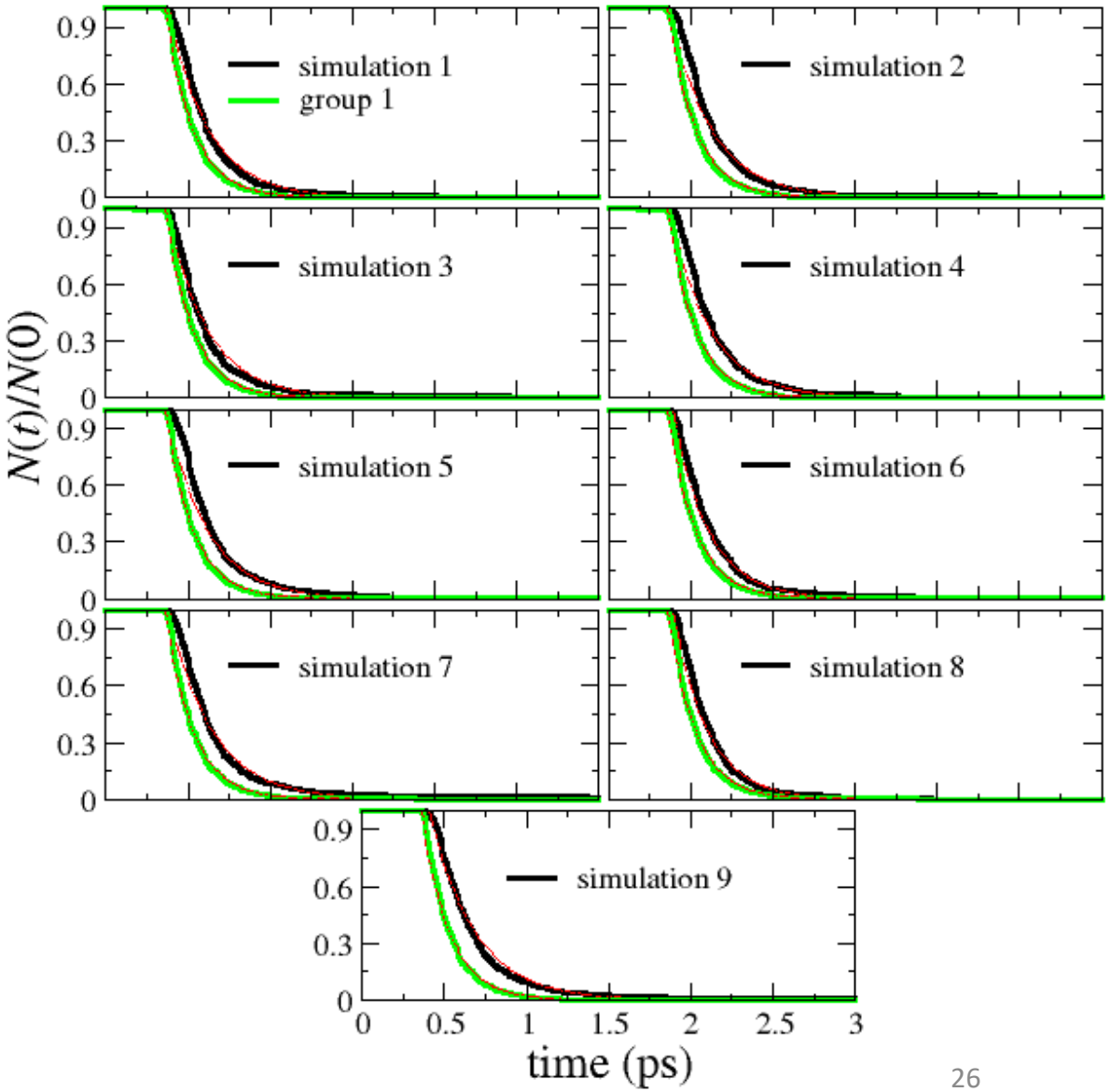

H. Mahanta, et al, *J. Phys. Chem. A* **2021**, *125*, 5870.

Normal Mode Analysis

$$H = \sum_k \frac{1}{2}\left({P_k}^2 + \lambda_k {Q_k}^2\right)$$

where P_k, and Q_k are the momentum and coordinate of k^{th} normal mode. $\lambda_k = 4\pi^2 \upsilon_k^2$, υ_k is the frequency of k^{th} normal mode. Cartesian q_i's and p_i's transferred to normal mode P_k's and Q_k's using normalized eigenvectors of the mass-weighted force constant matrix.

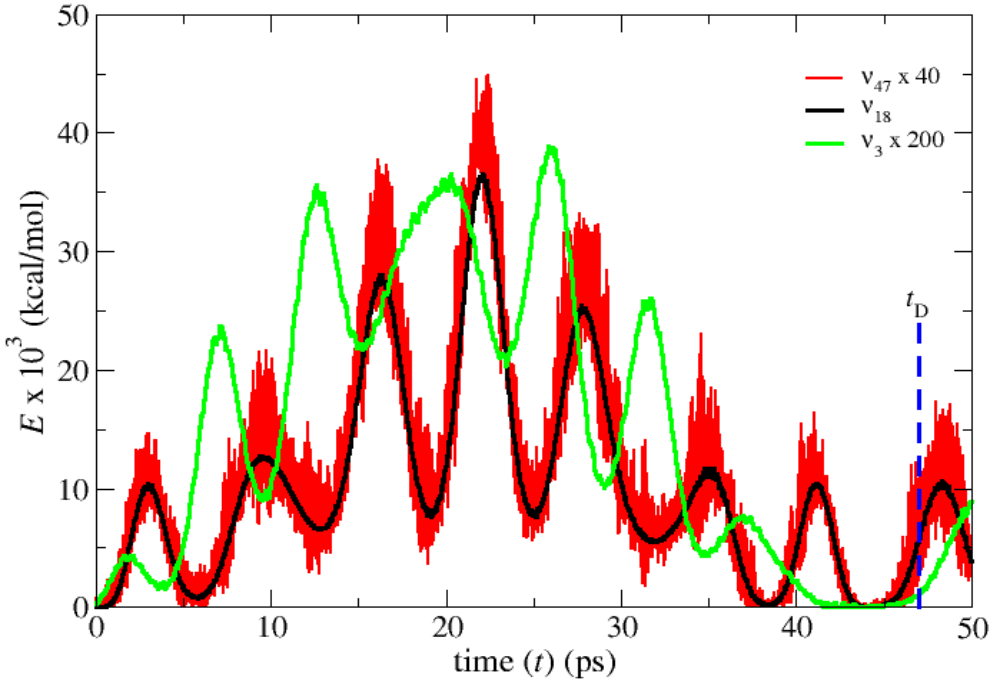

Abnormal Arrhenius Parameters of Bz-HCB

Arrhenius Equation: $k(T) = A\exp(-E_a/RT)$

Arrhenius Parameters: $\mathbf{E_a = 5.56\ kcal/mol}$, pre-exponential factor $\mathbf{(A) = 6.23 \times 10^{12}\ s^{-1}}$

Binding energy 9.14 kcal/mol

There could be some effect of anharmonicity on the Arrhenius parameters

Dissociating modes are 22.2 (x- directional motion), 22.2 (y- directional motion), and 71.1 cm^{-1}(z-directional motion)

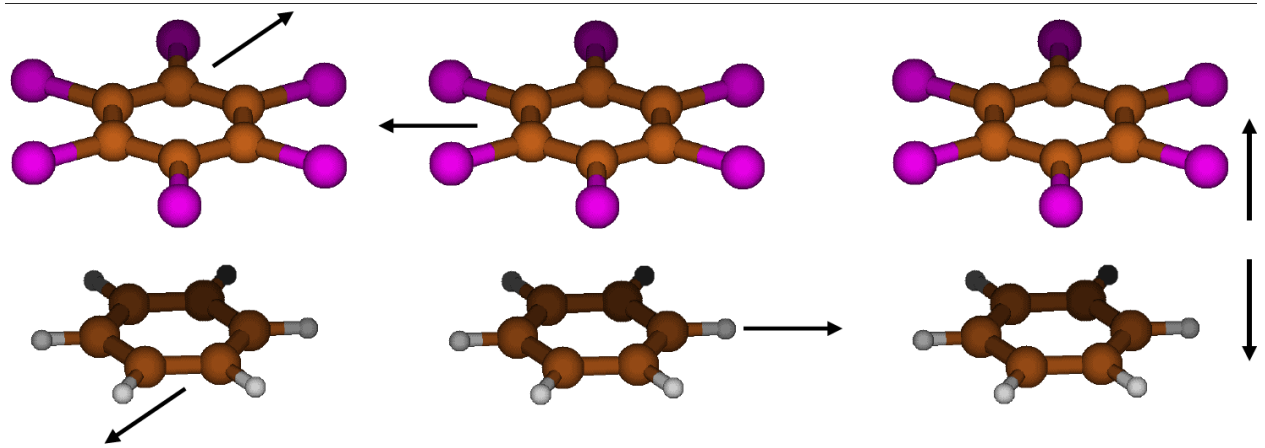

H. Mahanta, et al. Int. J. Mass. Spect. **2020**, 456, 116392.

Anharmonicity (Monte Carlo Model)

$$k_{anh}(T) = f_{anh}(T).\nu.\exp\left(-\frac{E_0}{k_B T}\right)$$

$$f_{anh}(T) = \frac{Q_h(T)}{Q_{anh}(T)}$$

$$Q(T) = \int_0^{\infty} \rho_{anh}(E) \exp\left(-E/k_B T\right) dE$$

$$Q_h(T) = \prod_{i=1}^{s} \frac{k_B T}{h\nu_i}$$

$$Q_{anh}(T) = \prod_{i=1}^{s-3} \frac{k_B T}{h\nu_i} \int_0^{\infty} \rho_{anh}(E) \exp\left(-E/k_B T\right) dE$$

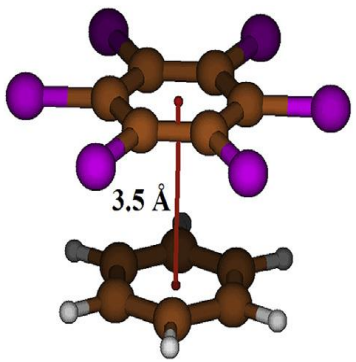

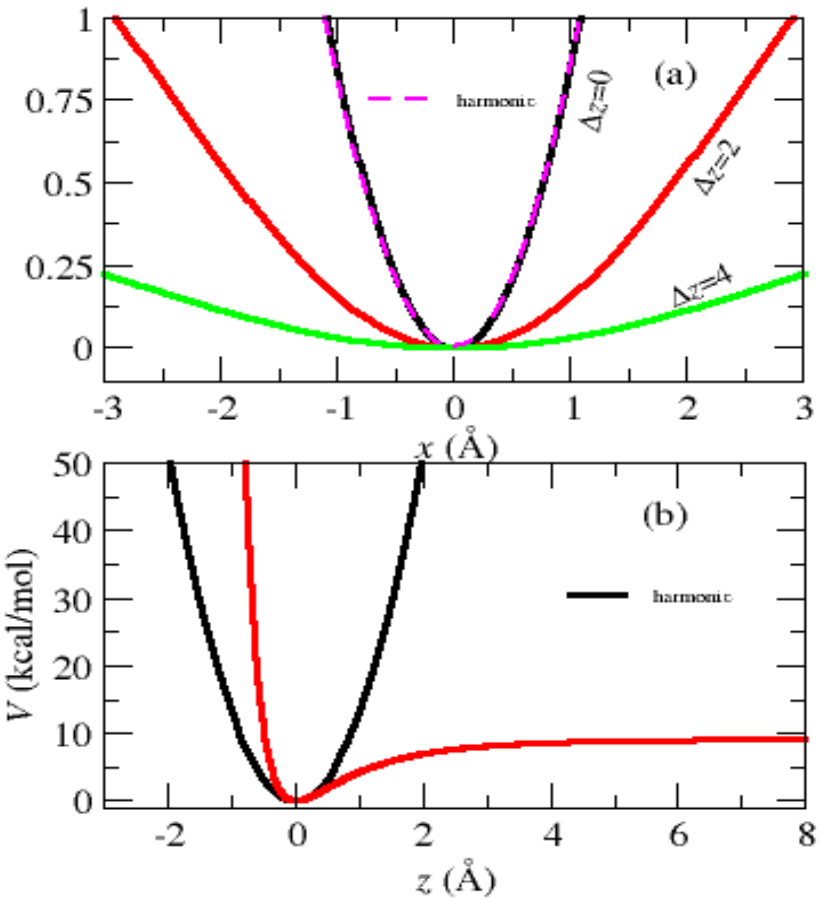

H. Mahanta, et al. Int. J. Mass. Spect. **2020**, 456, 116392.

Anharmonicity (Monte Carlo Model)

$$f_{anh}(T) = \frac{\prod_{i=1}^{3} \frac{k_B T}{h\nu_i}}{\int_0^{\infty} \rho_{anh}(E) \exp\left(-E/k_B T\right) dE}$$

Sum of states can be calculated from phase space integration

$$N(E) = 1/h^3 \iint_{H \le E} \dots\dots \int dqdp$$

$$\rho(E) = \frac{dN(E)}{dE}$$

Hamiltonian

$$H = \frac{p_{Q_x}^2}{2\mu_{Q_x}} + \frac{p_{Q_y}^2}{2\mu_{Q_y}} + \frac{p_{Q_z}^2}{2\mu_{Q_z}} + V\left(q_{Q_x}, q_{Q_y}, q_{Q_z}\right)$$

$$\nu_i\ (s^{-1}) = \frac{1}{2\pi}\sqrt{\frac{f_i}{\mu_i}}$$

H. Mahanta, et al. Int. J. Mass. Spect. **2020**, 456, 116392.

Anharmonicity (Phase space)

$V(0,0,Z_{max})$ = 9.14 kcal/mol

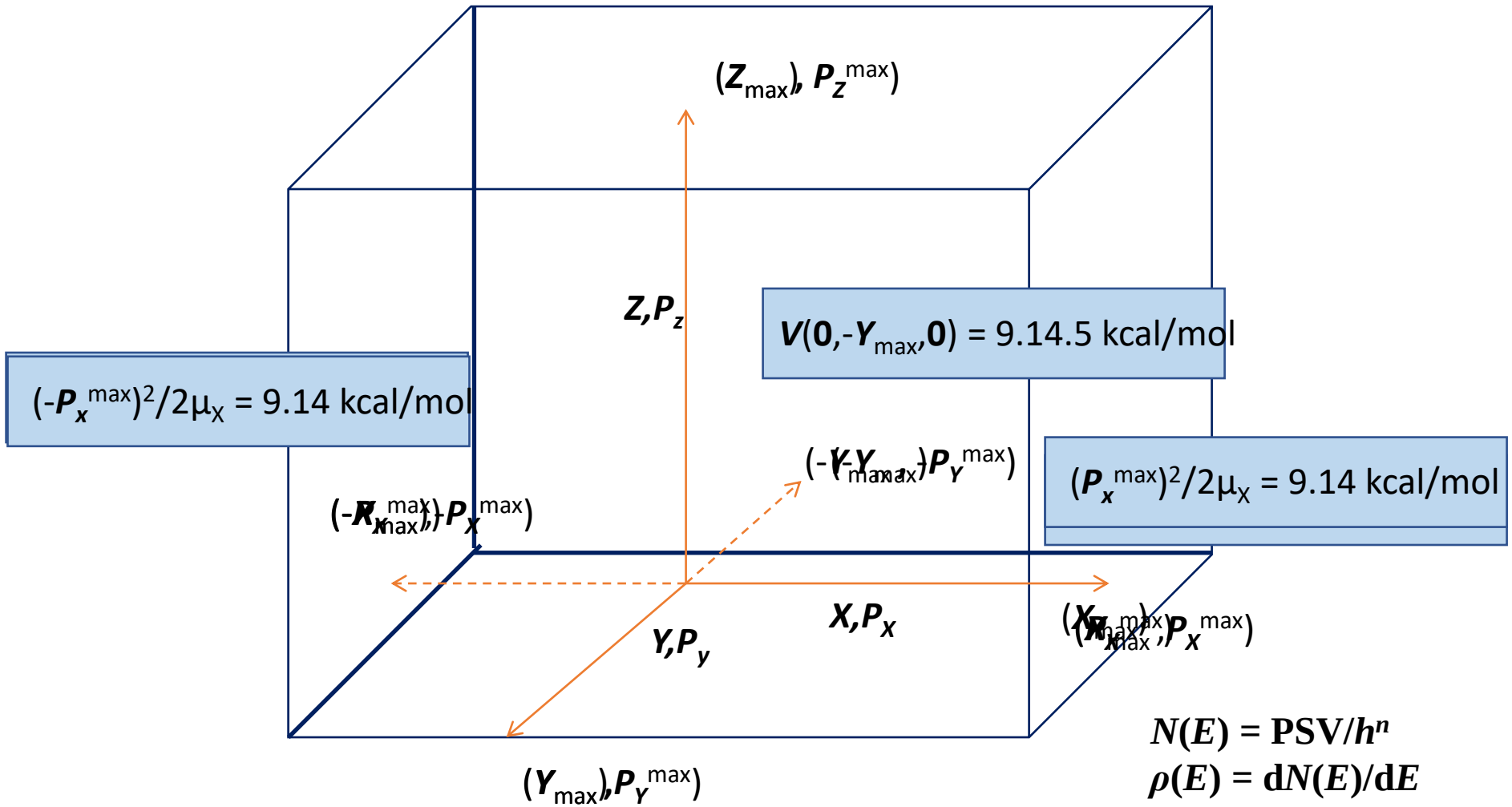

$V(0,Y_{max},0)$ = 9.14 kcal/mol

$$N(E) = \mathrm{PSV}/h^n$$
$$\rho(E) = \mathrm{d}N(E)/\mathrm{d}E$$

H. Mahanta, et al. Int. J. Mass. Spect. **2020**, 456, 116392.

Harmonic vs anharmonic sum of states

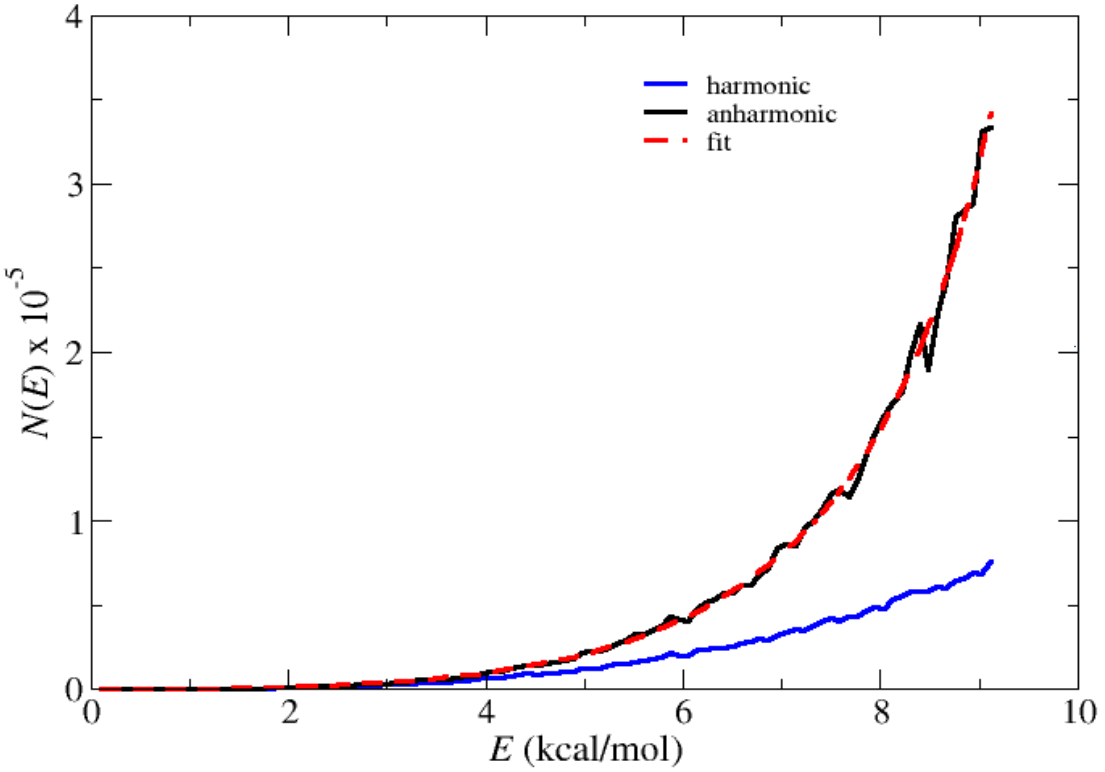

Arrhenius Parameters: $\mathbf{E_a = 9.14\ kcal/mol}$, pre-exponential factor $\mathbf{(A) = 1.05 \times 10^{14}\ s^{-1}}$

H. Mahanta, et al. Int. J. Mass. Spect. **2020**, 456, 116392.

$$k_{anh}(T) = f_{anh}(T).\nu.\exp\left(-\frac{E_0}{k_B T}\right)$$

An analytic form of temperature dependent anharmonic factor was also considered as $exp(-bT^d)$ as used previously. This leads to a modified Arrhenius equation:

$$\ln\big(k(t_0,T)\big) = -bT^d + \ln\upsilon - \frac{E_0}{k_B T}$$

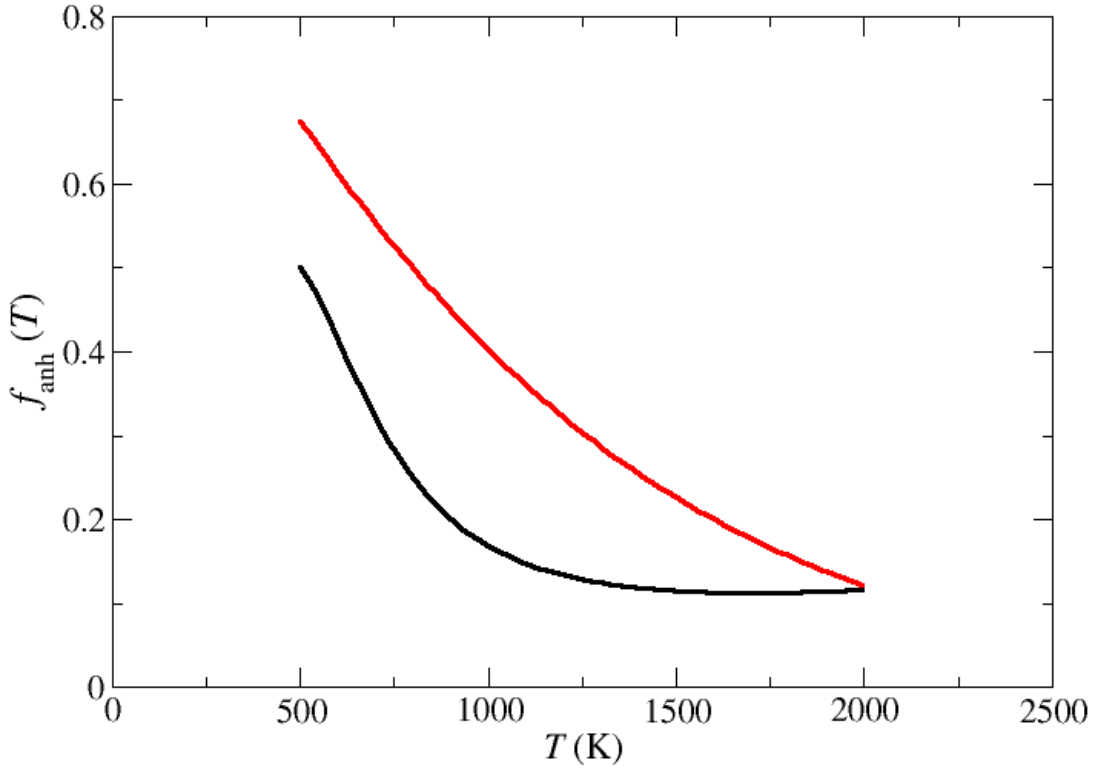

exp($-bT^d$) (red) and from Monte Carlo method (black)

H. Mahanta, et al. Int. J. Mass. Spect. **2020**, 456, 116392.

Bz-HFB-Bz

Partial Dissociation

T(K)	f_1	f_2	k_1	k_2	$k(t_0)^a$	$k(t_0)^{19}$
1000	0.87	0.13	1.60	0.28	1.43	1.02
1200	0.89	0.11	1.89	0.96	1.79	1.43
1500	0.90	0.10	2.80	1.40	2.66	2.09
1800	0.92	0.08	3.00	2.30	2.94	2.44
2000	0.94	0.06	4.10	2.70	4.02	2.94

Complete Dissociation

T(K)	f_1	f_2	k_1	k_2	$k(t_0)$
1000	0.28	0.72	0.70	0.14	0.30
1200	0.57	0.43	0.87	0.15	0.56
1500	0.70	0.30	0.95	0.20	0.73
1800	0.75	0.25	1.30	0.24	1.04
2000	0.80	0.20	1.48	0.24	1.23

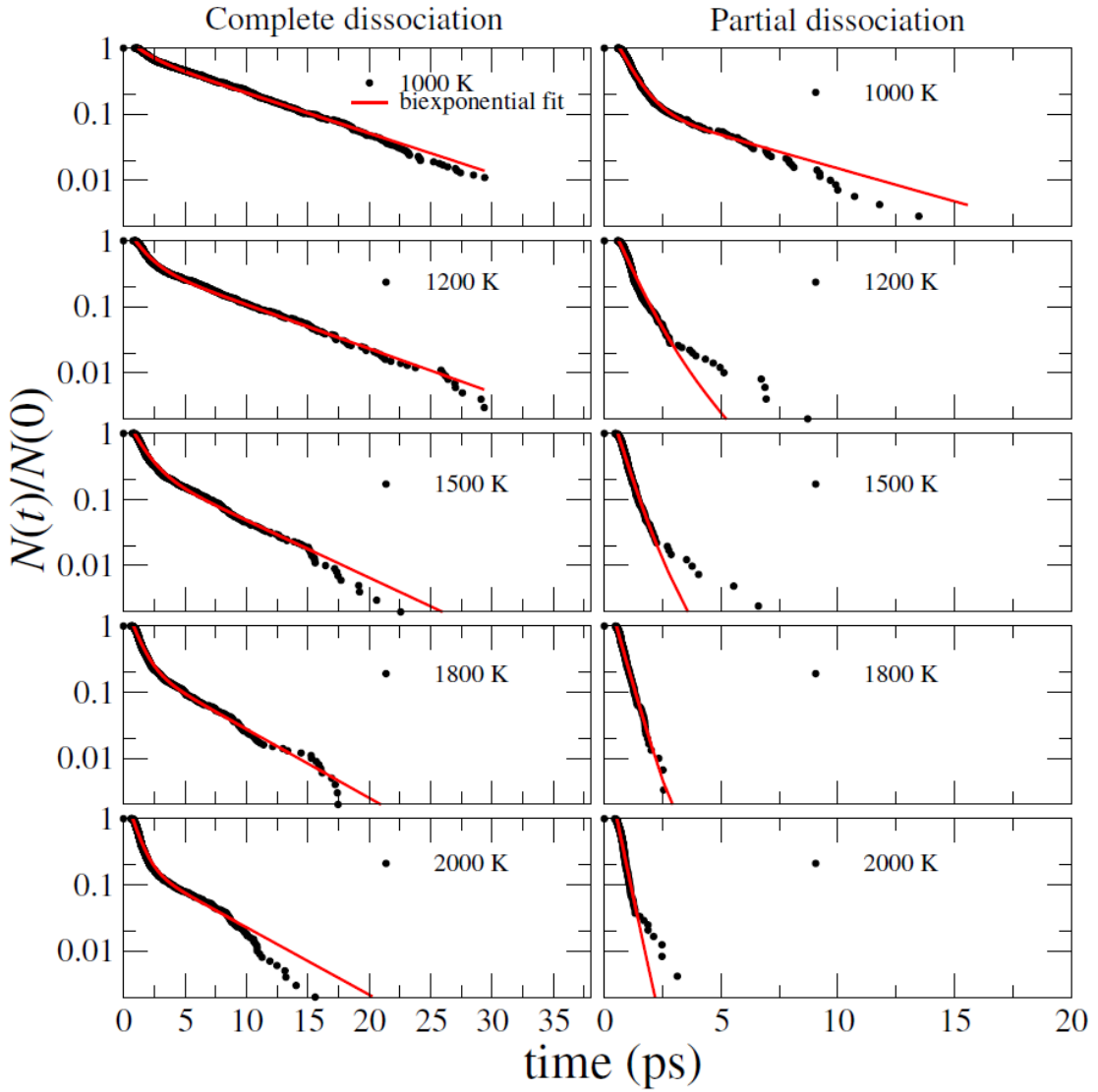

Bz-trimer

Partial Dissociation

T(K)	f_1	f_2	k_1	k_2	$k(t_0)^a$	$k(t_0)$ [21]
1000	0.55	0.45	2.10	0.90	1.56	0.881
1200	0.58	0.42	2.20	1.45	1.89	1.025
1500	0.59	0.41	2.40	1.68	2.11	1.239
1800	0.62	0.38	2.95	2.40	2.74	—
2000	0.63	0.37	3.10	2.10	2.73	—

Complete Dissociation

T(K)	f_1	f_2	k_1	k_2	$k(t_0)$
1000	0.82	0.18	0.79	0.17	0.68
1200	0.83	0.17	0.99	0.19	0.85
1500	0.89	0.11	1.32	0.25	1.20
1800	0.95	0.05	1.55	0.20	1.48
2000	0.94	0.06	1.58	0.25	1.50

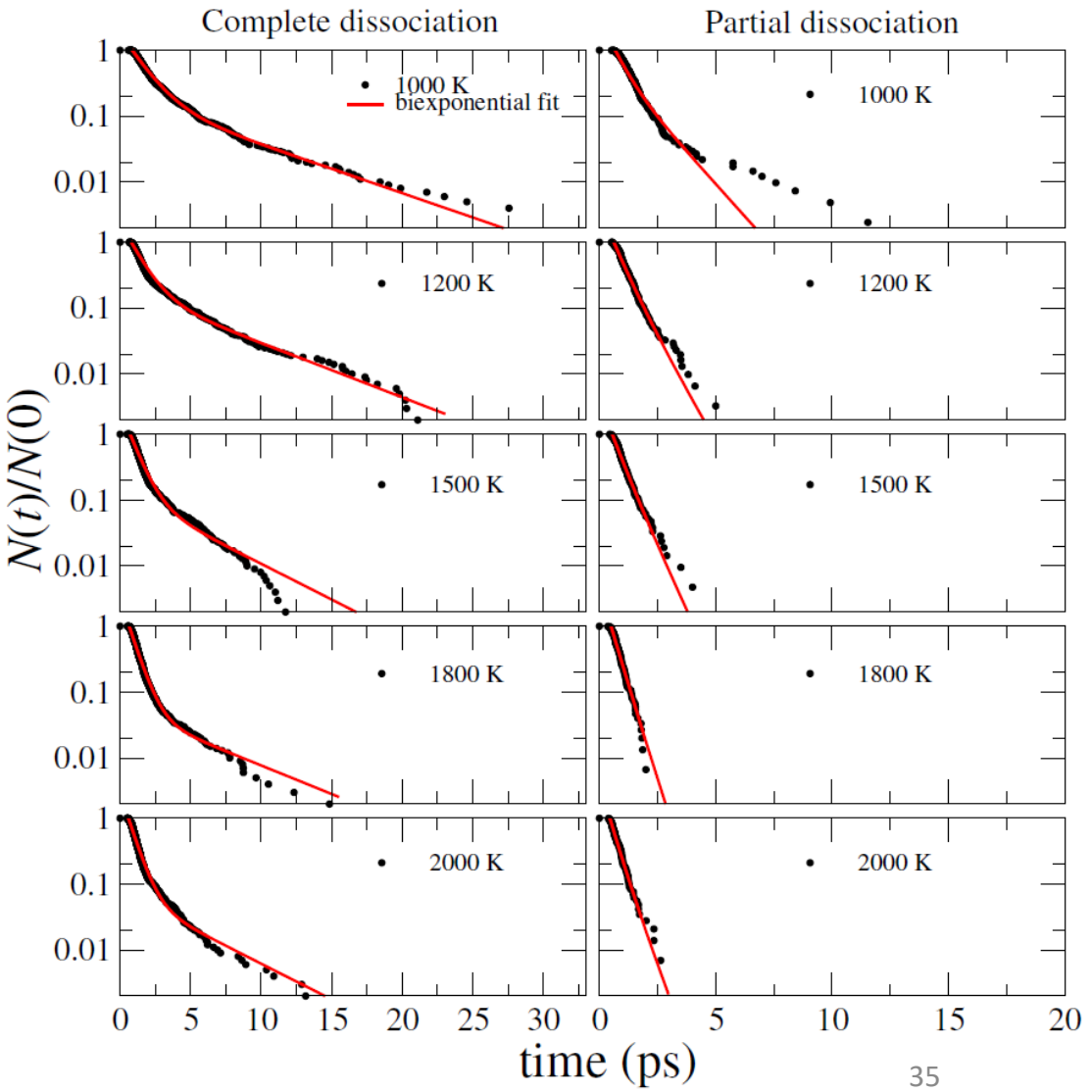

Application

- Association Followed by Ensuing Dissociation Dynamics

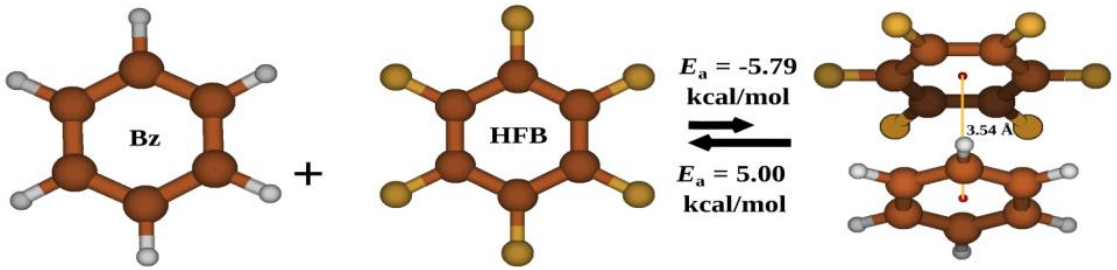

Simulation Methodology

- The chemical dynamics simulations are performed to study the association of Bz and HFB followed by ensuing dissociation at temperatures 1000, 1500, and 2000 K with collision impact parameter (b) 0-10 Å at each temperature.
- Quasiclassical microcanonical normal mode sampling is considered to choose initial p's and q's.
- The average quantum vibrational energies are calculated for these simulations using harmonic oscillator equation.
- At 1500 K, four different center-of-mass translational energies, i.e., 2.0, 4.5, 7, 9.5 kcal/mol are considered as the initial collision energy to obtain temperature-dependent association rate constant.
- A total of 1000 trajectories are integrated for a maximum of 30 ps using 6^{th} order symplectic integrator for each temperature and impact parameter.
- All calculations are done in VENUS, a chemical dynamics computer program.

Result and Discussion

Association of Bz and HFB complex

- Trajectory Types

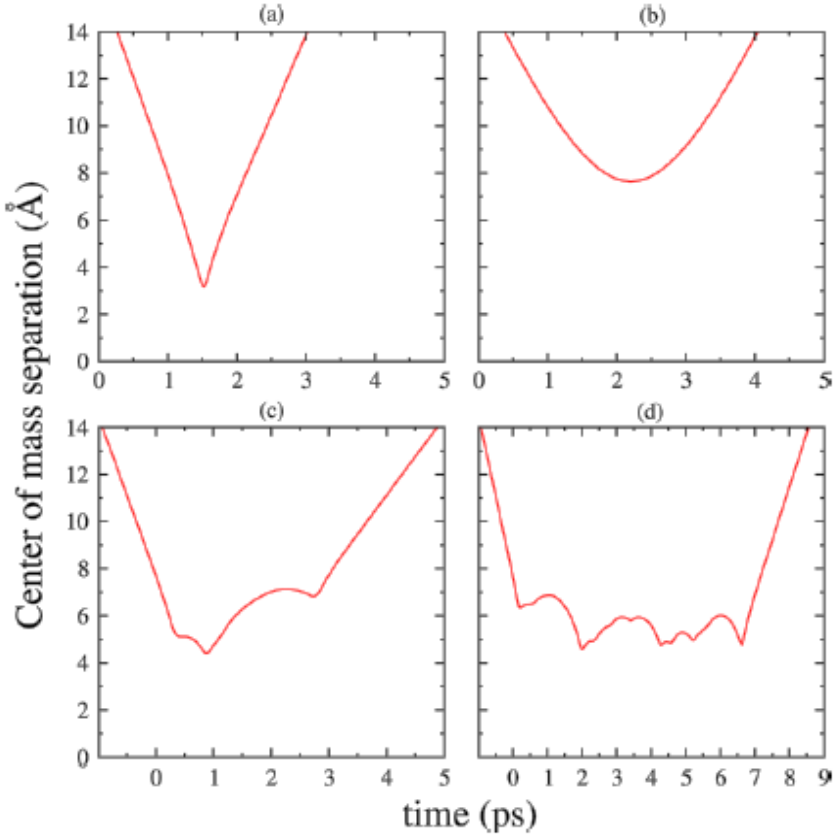

Different types of trajectories for complex formation.

Association Probability

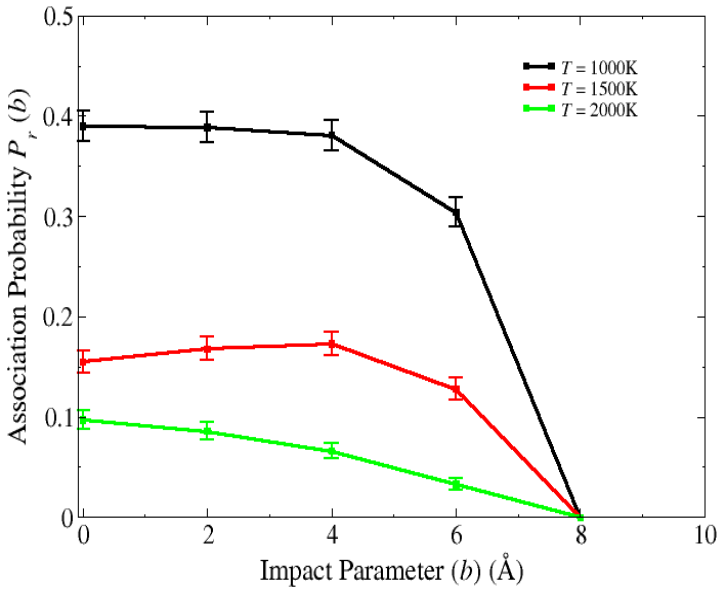

Association probabilities as obtained at 1000, 1500, and 2000 K simulations versus impact parameter (*b*)

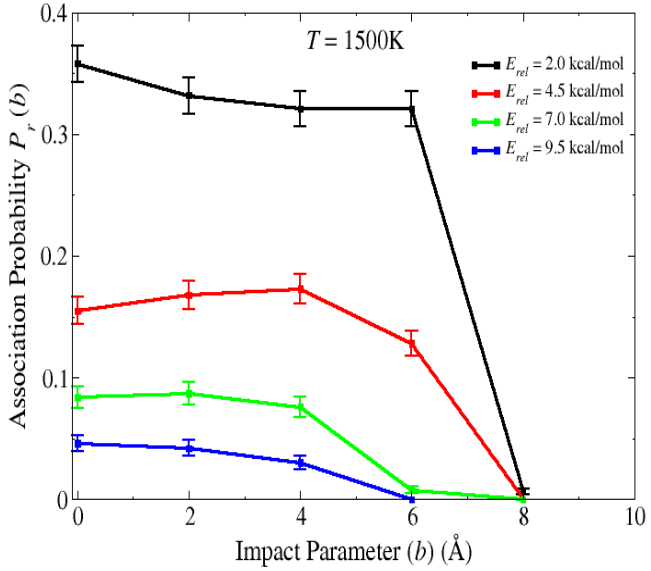

Association probability versus impact parameter (b) at 1500K for three relative energies 2.0, 4.5, 7.0,and 9.5 kcal/mol

- A maximum probability of ~0.4 ± 0.02, ~0.15 ± 0.01, ~0.1 ± 0.01 are obtained for simulation at 1000 K, 1500 K and 2000 K, respectively with b = 0, 2, and 4 Å.
- Association probability decreased with the increased temperatures

Association Rate Constant $k_{asso}(T)$

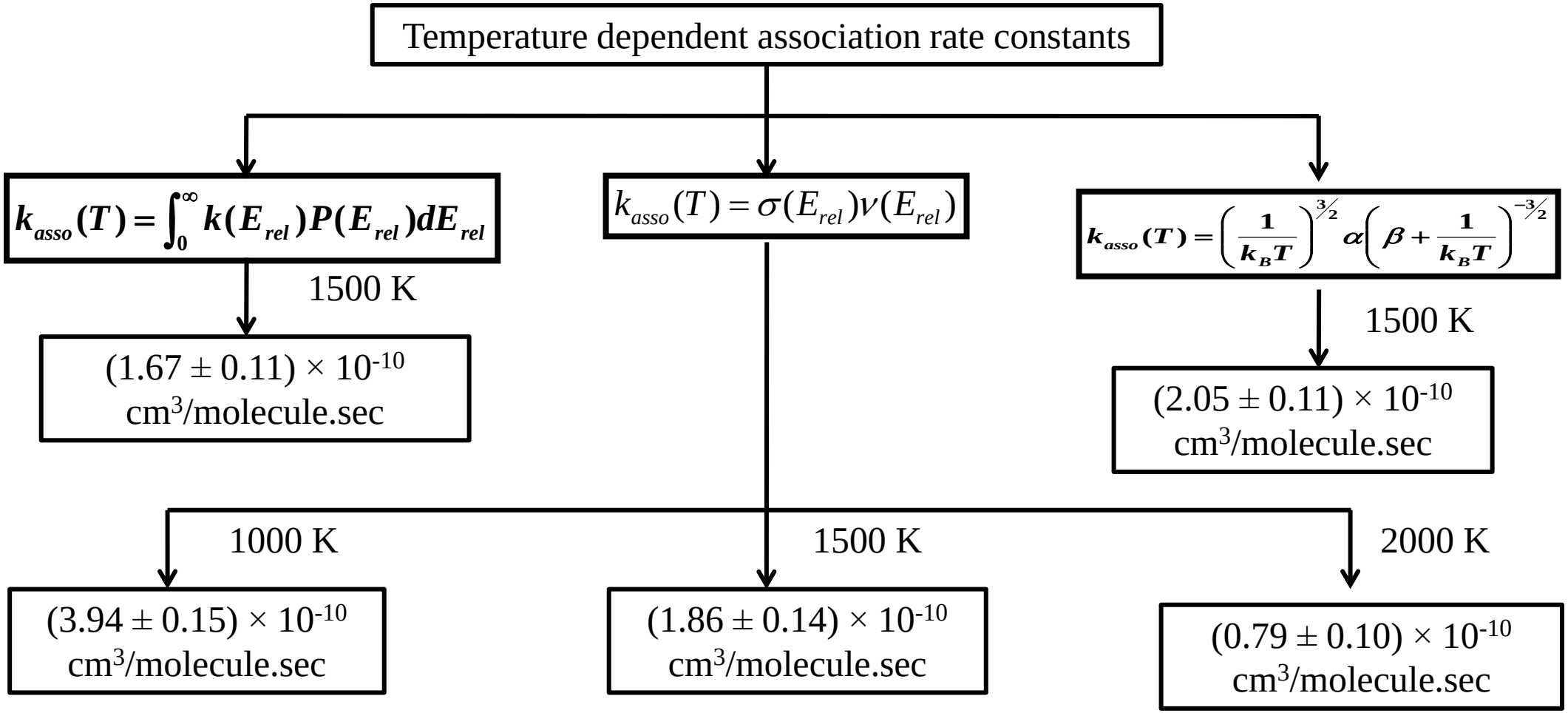

- $k(E_{rel})$ is calculated as

$$k(E_{rel}) = \sigma(E_{rel})v(E_{rel})$$

- Association rate constants decreased with the increased temperatures

Association Followed by Ensuing Dissociation Dynamics

- The calculated $k(E_{rel})$ values are fit in to

$$k(E_{rel}) = \alpha . \exp(-\beta . E_{rel})$$

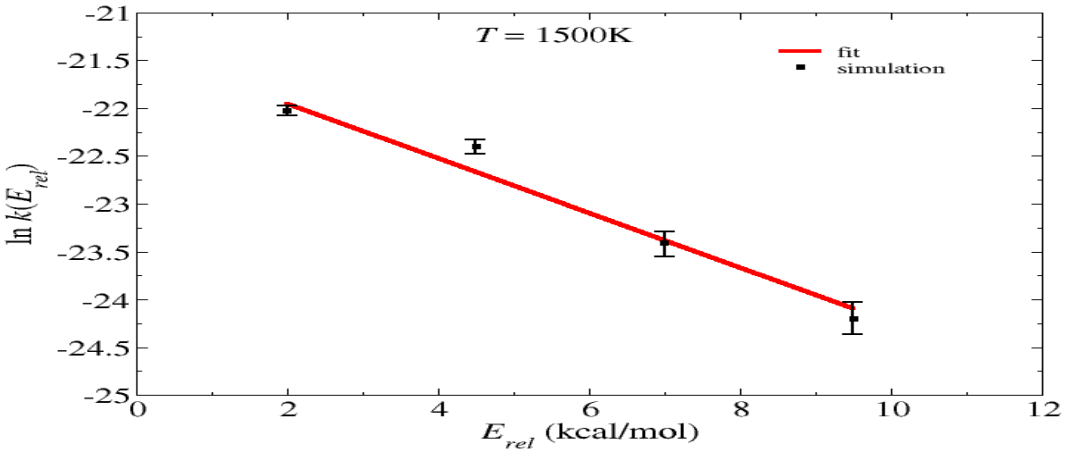

Figure 6 .4 ln $k(E_{rel})$ versus E_{rel} for the simulation at 1500 K

Arrhenius equation

$$\ln k_{asso}(T) = \ln A - \frac{E_a}{RT}$$

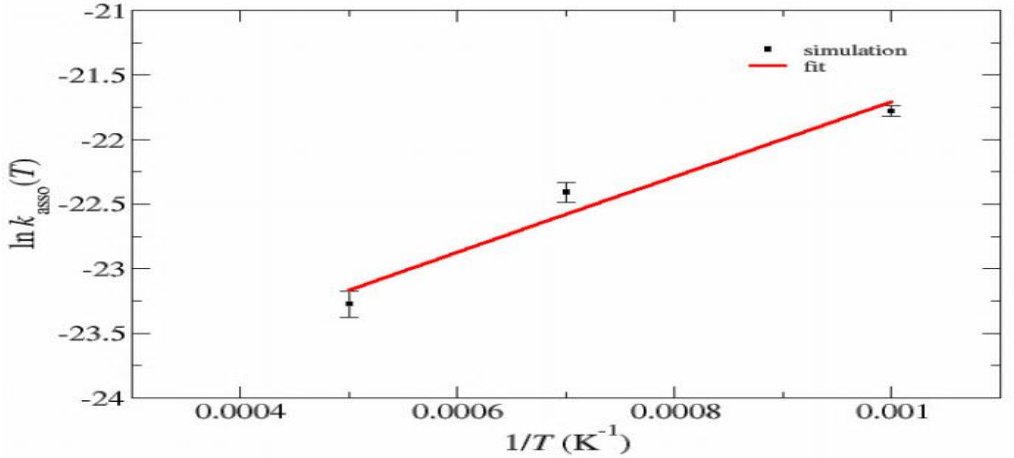

Figure 6.5 ln k_{asso}(T) versus 1/T.

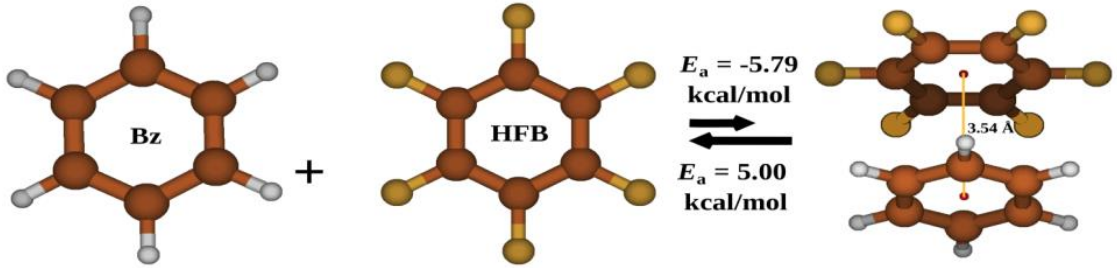

$\alpha = 5.17 \times 10^{-10}$ cm^3/molecule·s
$\beta = 0.29$ (kcal/mol)$^{-1}$

$\nu = 10.91 \times 10^{-12}$ s^{-1} (unimolecular dissociation)
$\nu = 0.203 \times 10^{-10}$ cm^3/molecule·s (association)

Ensuing Dissociation

- The relative numbers of undissociated trajectories

$$\frac{N(t)}{N(0)} = e^{-k(t_0)(t-t_0)}$$

Table 5.1 The Fit Parameters of $N(t)/N(0)$ of Ensuing Dissociation

T (K)	Impact Parameter, b (Å)	k (ps^{-1})	t_0 (ps)
1000	0.0	0.48	1.85
	2.0	0.47	1.85
	4.0	0.58	1.85
	6.0	0.89	1.95
1500	0.0	0.41	1.95
	2.0	0.50	1.85
	4.0	0.65	1.85
	6.0	2.20	1.98
2000	0.0	0.43	1.85
	2.0	0.46	1.75
	4.0	0.88	2.05
	6.0	7.20	2.00

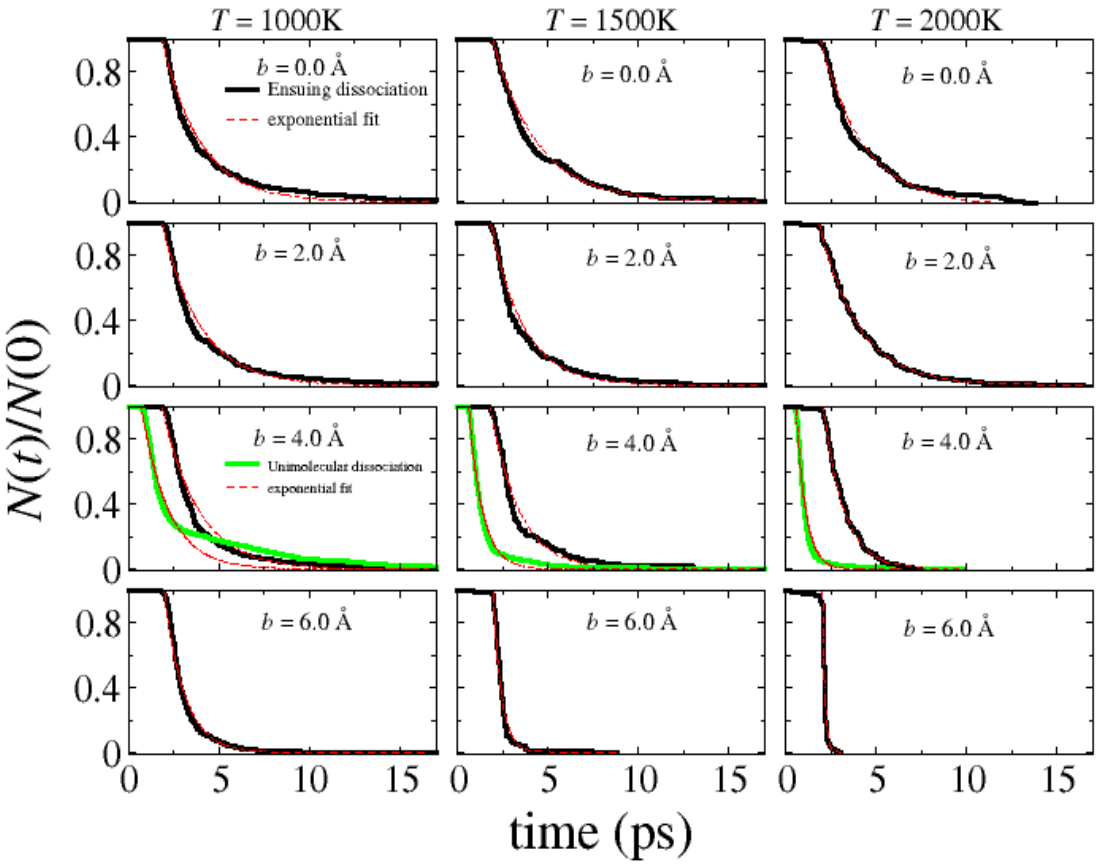

Figure 6.6 $N(t)/N(0)$ of ensuing dissociation versus time for b = 0, 2, 4 and 6 Å at 1000, 1500 and 2000 K. In the panel b = 4 Å unimolecular dissociation is also presented .

Comparison ensuing dissociation dynamics with unimolecular dissociation of Bz-HFB

Parameters	Unimolecular dissociation	Ensuing dissociation
$N(t)/N(0)$	Fitted biexponentially	Fitted exponentially
Dissociation nature	Temperature independent at b= 0 and 2 Å	Temperature dependent

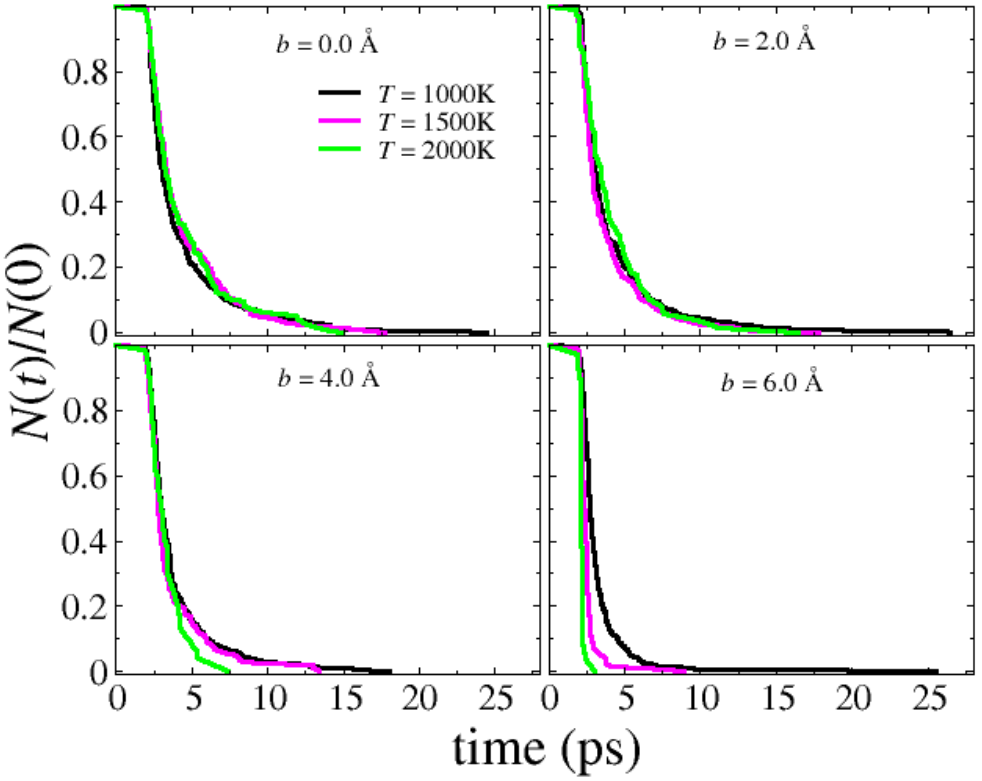

Figure 6.7 $N(t)/N(0)$ of the ensuing dissociation of Bz-HFB complex versus time at 1000 ,1500 and 2000K for each b = 0, 2, 4, and 6 Å

Application

- Simulation in Condensed Phases

Motivation

• Non bonded interactions among aromatic molecules are important in

1. Crystal Engineering
2. Supramolecular Chemistry
3. Combustion Chemistry

etc.

• In combustion chemistry, detail understanding of the dynamical behaviour of such complexes is crucial for understanding the interaction pattern

• The aggregation of PAH molecules at very high combustion temperature is known to be the precursor of soot formation. It may be noted that the binding energy for aromatic complexes is low.

• Moreover, since the association and/or dissociation of aromatic molecules are environmentally relevant, role of the surrounding molecules is also crucial to know.

44

Potential Energy

- $V = V_{intramolecular} + V_{intermolecular}$
- $V_{intramolecular} = \sum V_{solute} + \sum V_{solvent}$
- $V_{intermolecular} = \sum V_{solute-solute} + \sum V_{solute-solvent} + \sum V_{solvent-solvent}$

In the case of vacuum calculation, Potential energy terms for the solvent are missing

$C_6H_6 + C_6H_6$ in N_2 Bath

$$V = \underbrace{V_{C_6H_6} + V_{N_2}}_{\text{Intramolecular}} + \underbrace{V_{C_6H_6-C_6H_6} + V_{N_2-N_2} + V_{C_6H_6-N_2}}_{\text{Intermolecular}}$$

$$V_{C_6H_6-C_6H_6}/V_{C_6H_6-N_2}/V_{N_2-N_2} = \sum_i \sum_j V_{ij}$$ where i, j are atom index

OPLS-AA parameters were used for C_6H_6-C_6H_6 interactions

$$V_{C_i-N_j} = \sum_i \sum_j A_{C-N} e^{-B_{C-N} r_{ij}} + \frac{C_{C-N}}{r_{ij}^n} + \frac{D_{C-N}}{r_{ij}^m}$$

$$V_{H_i-N_j} = \sum_i \sum_j A_{H-N} e^{-B_{H-N} r_{ij}} + \frac{C_{H-N}}{r_{ij}^n} + \frac{D_{H-N}}{r_{ij}^m}$$

$$V_{N_i-N_j} = \sum_i \sum_j A_{N-N} e^{-B_{N-N}(r_{ij}-b)} + \frac{C_{N-N}}{(r_{ij}+c)^n} + \frac{D_{H-N}}{(r_{ij}+d)^m}$$

J. Phys. Chem. A **2015**, *119*, 6631
J. Chem. Phys. **2014**, *140*, 194103,
J. Chem. Phys. **2018**, *149*, 134101

System Preparation

Reactant System

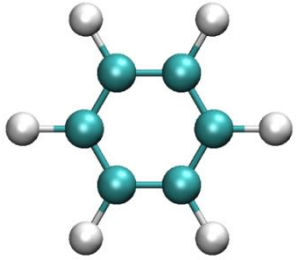

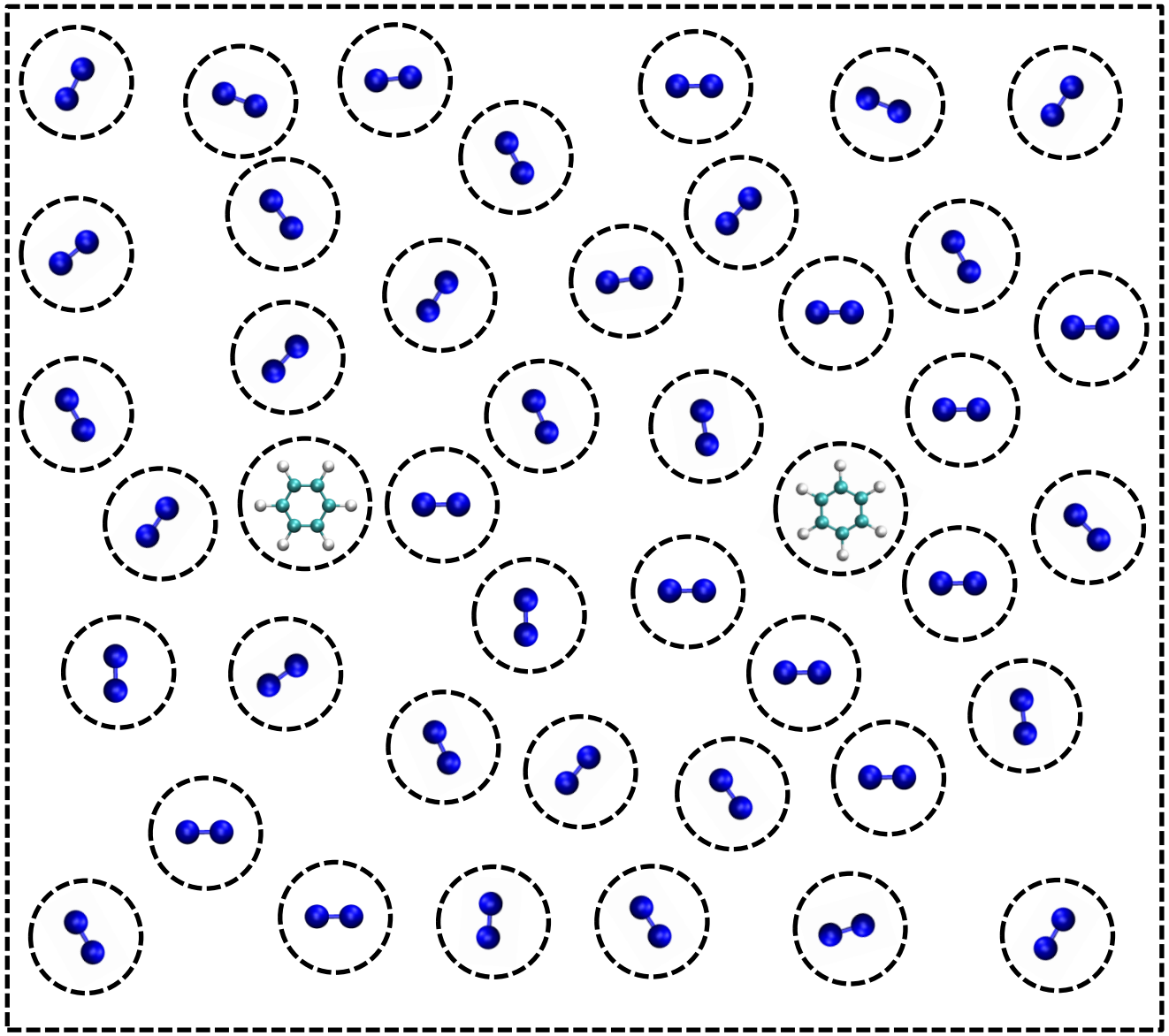

Solvent

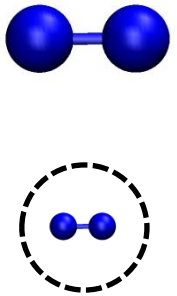

Initial Conditions

Reactants, C_6H_6 + C_6H_6

- The initial vibration excitation energy is taken as the quantum vibrational energy at temperatures 1000, 1500, and 2000 K for each of the benzenes.
- This energy is sampled among 30 modes of each of C_6H_6 using *microcanonical normal mode* sampling.
- Initial benzene – benzene distance is taken as 16 Å and a relative kinetic energy of 3/2 RT is added where T is the bath temperature and an impact parameter range of 0-12 Å is considered
- Initial COM Translational and Rotational energy of C_6H_6 is sampled from a Boltzmann distribution at bath temperature.

Solvent, N_2

- Initial Momentum is assigned to each DOF of each atom by selecting 1-d velocity (v_x, v_y and v_z) from a Boltzmann distribution at 298 K temperature.
- The Boltzmann probability distribution $P(\Delta r) \propto \exp(-k\Delta r^2/2k_BT)$ of the N_2 potential energy is sampled for each N_2 molecule to determine its bond length.
- Bath densities of 20 kg/m^3 as well as 324 kg/m^3 are considered

Equilibration

Stage 1

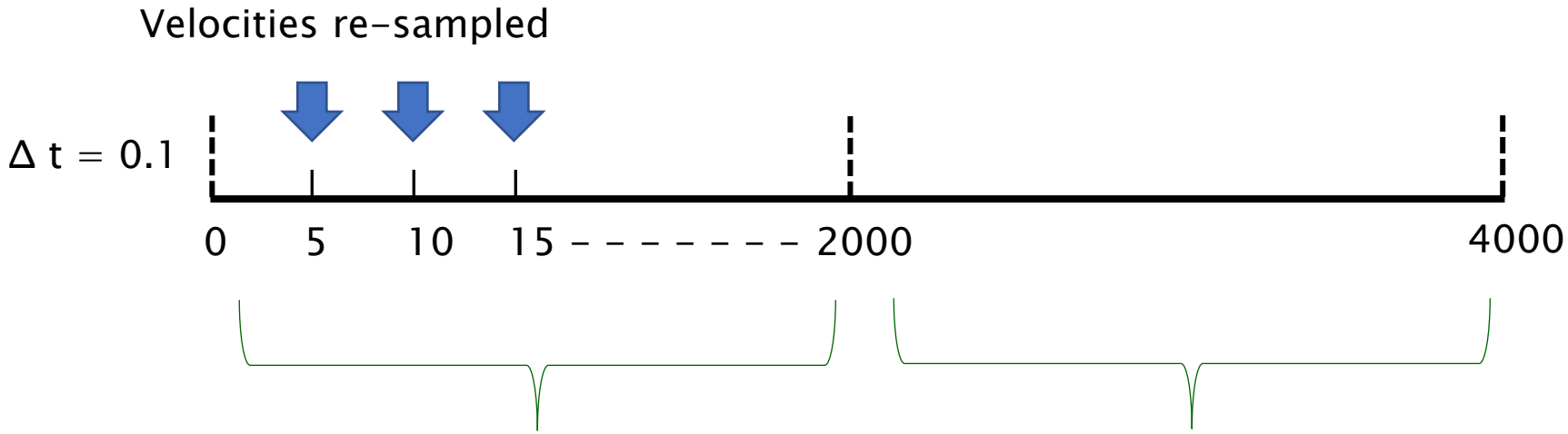

- Temperature is calculated at each step
- Velocities are re-sampled after certain number of steps

- Effectiveness of sampling phase is tested
- Monitored:
  - Temperature
  - Radial Distribution Function
  - Energy conservation

Equation of motion for the solute is not solved

Equilibration

➢During equilibration properties are monitored

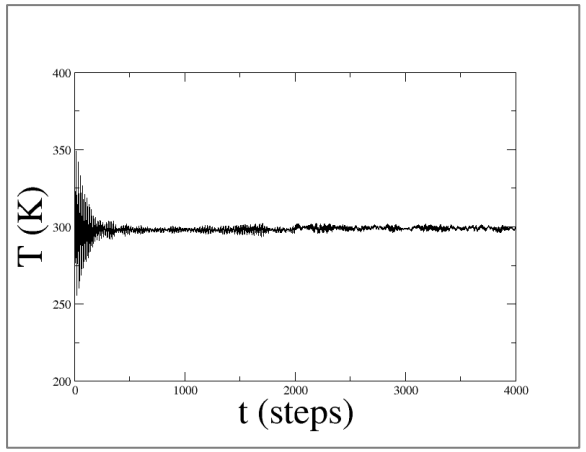

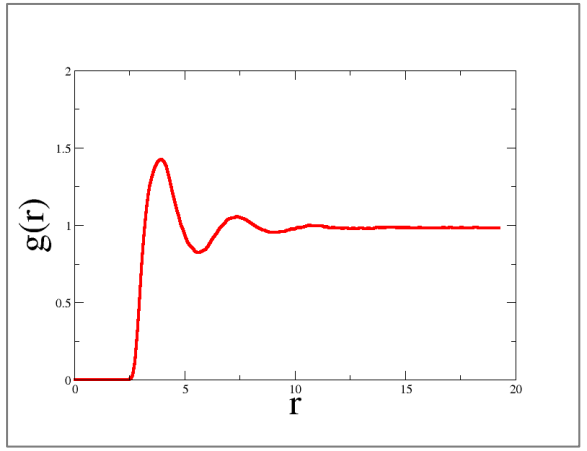

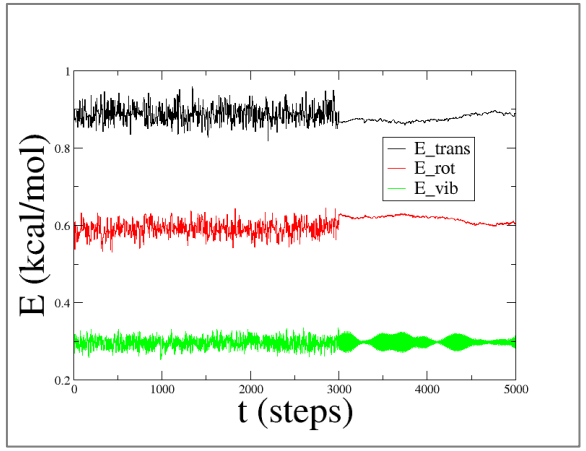

- Temperature
- Radial Distribution Function
- Energy Components
  - Translational, 3RT/2 = 0.9 kcal/mol at 300 K
  - Rotational, RT = 0.6 kcal/mol
  - Vibrational, RT/2 = 0.3 kcal/mol

Steps of Molecular Dynamics

The system under investigation is chosen

↓

Utilizing accurate force filled parameter for the interacting system

↓

Preparation of simulation box

↓

Initial sampling of the molecules

↓

Equilibration

↓

Trajectory runs

Single Bath

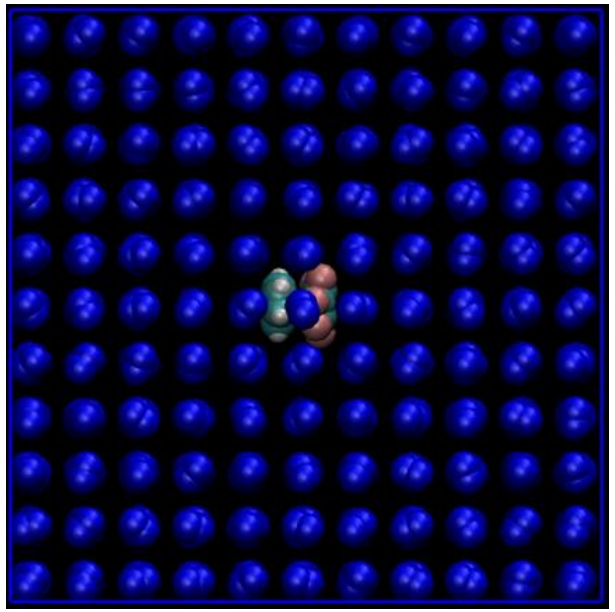

Mixed Bath

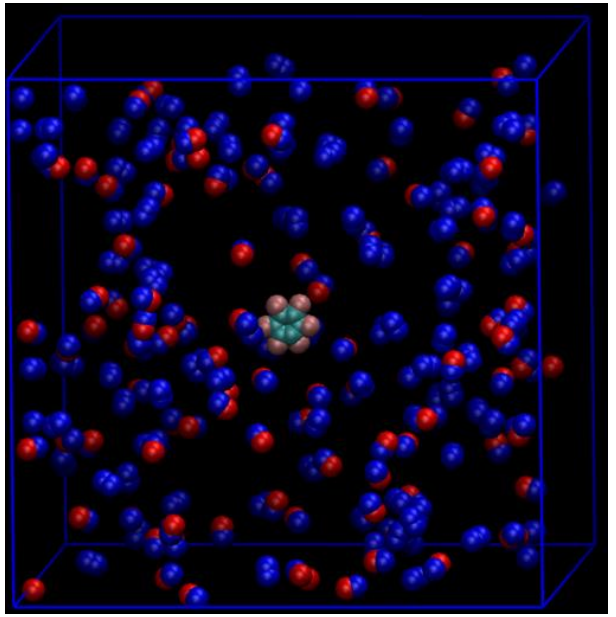

Dissociation/Association Versus Energy Transfer in N2 Bath

Unimolecular Dissociation of Bz-HFB complex and Effect of Energy Transfer

- ✓ The unimolecular dissociation of Bz-HFB are performed in a N_2 bath with 1000 N_2 molecules.
- ✓ CIET from vibrationally excited Bz-HFB to N_2 bath is studied simultaneously.
- ✓ The dissociation of the complex is studied at three different N_2 bath densities of 20, 324, and 750 kg/m^3.
- ✓ Three different initial temperatures of Bz-HFB complex as 1000, 1500, and 2000 K are considered here.
- ✓ The total integration times are 25, 25 and 50 ps for the bath densities of 20, 324, and 750 kg/m^3 for most of the trajectories.
- ✓ 75 trajectories are integrated for each temperature for a particular density.

Potential Energy

- The overall potential energy for any system can be expressed as

$$V = V_{intra} + V_{inter}$$

- The potential energy function for Bz-HFB + N_2-bath system is written as

$$V = V_{Bz} + V_{HFB} + V_{N_2} + V_{Bz-HFB} + V_{N_2-Bz} + V_{N_2-HFB} + V_{N_2-N_2}$$

- V_{Bz}, V_{HFB}, and V_{N_2} are the intramolecular potential energies of benzene, hexafluorobenzene, and nitrogen, respectively.

- $V_{Bz\text{-}HFB}$, V_{N_2-Bz}, V_{N_2-HFB}, and $V_{N_2-N_2}$ are the intermolecular potential energies for Bz and HFB, N_2 and Bz, N_2 and HFB, and N_2 and N_2, respectively.

- The potential energy used in this work are taken from literature.

- All the potentials are very authentic and used several times in past.

Simulation Method

- The simulations are performed using Venus Chemical Dynamics Computer Programme implemented with condensed phase algorithms.

- The lengths of the simulation box are 133.2, 54.18, and 42.50 Å at the bath densities of 20, 324, and 750 kg/m3, respectively.

- The sampling method used here is quasiclassical microcanonical normal mode sampling.

$$E_{vib} = N \sum_{i=1}^{s} \left(\frac{h\nu_i}{2} + \frac{h\nu_i}{e^{\frac{h\nu_i}{k_B T}} - 1} \right)$$

- The corresponding energies at 1000, 1500, and 2000 K are 164.6, 220.8, and 280.9 kcal/mol.

- The bath temperature is kept 300 K.

- In the sampling phase of the equilibration, the velocities of each N atom is rescaled at every 5 integration step.

- The equilibration is done for 150-168 ps.

Analysis of the Trajectory Results

1. Rate of dissociation: The rate of dissociation of the complex is measured from the relative number of undissociated trajectory with time by fitting bi and single exponential equation as

$$\frac{N(t-t_0)}{N(t_0)} = f_1 exp\big(-k_1(t-t_0)\big) + f_2 exp\big(-k_2(t-t_0)\big) \tag{4.4}$$

$$\frac{N(t-t_0)}{N(t_0)} = exp\big(-k(t-t_0)\big) \tag{4.5}$$

2. Energy Transfer: The energy transfer rate of the complex is obtained from bi-exponential equation as

$$\langle E(t)\rangle = (\langle E_0\rangle - E_\infty) \times \left[\tilde{f}_1\, exp\big(-\tilde{k}_1 t\big) + \tilde{f}_2\, exp\big(-\tilde{k}_2 t\big)\right] + E_\infty \tag{4.6}$$

Where k_1, k_2 are rate constant and f_1, f_2 are coefficient.

Simulation Results

➢ Dissociation Phenomena

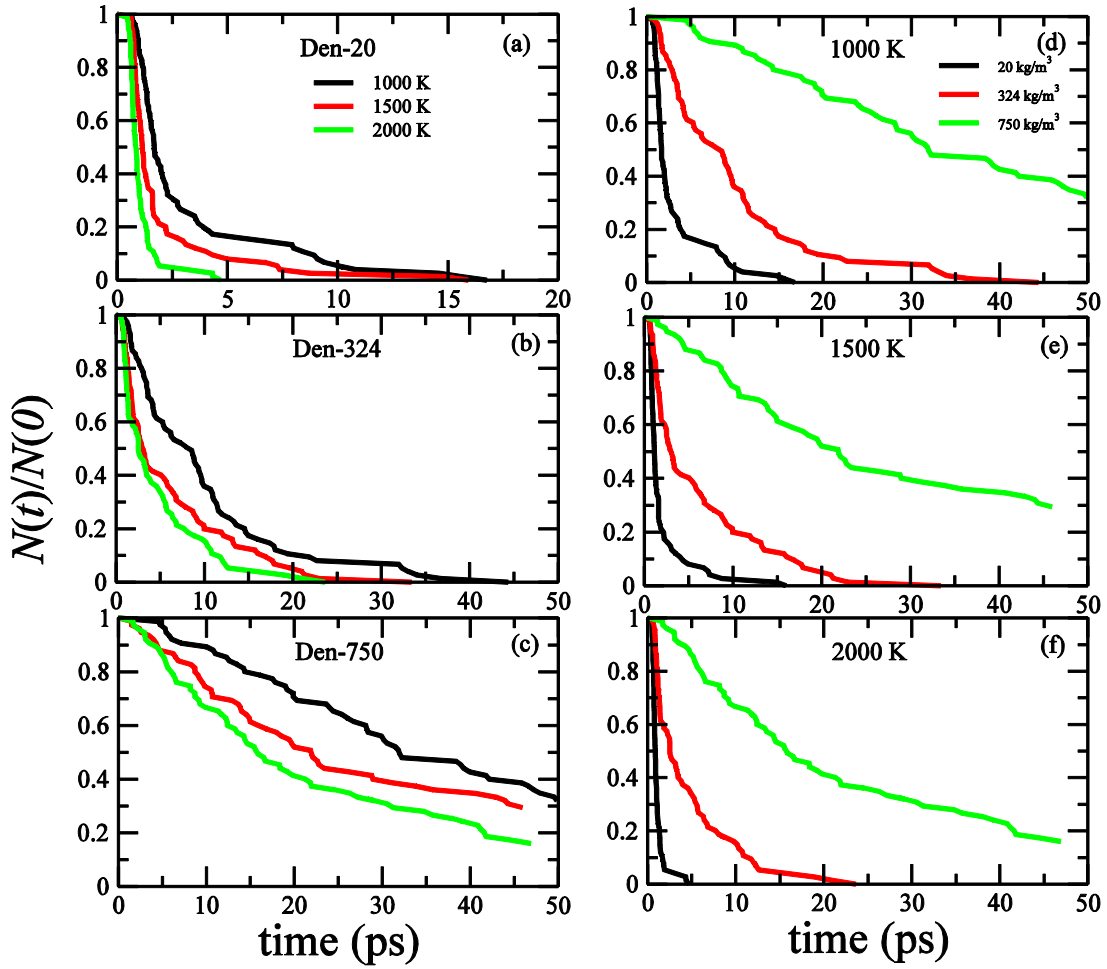

- ✓ There is a significant time lag(t_0) before starting the dissociation.
- ✓ Higher the bath density lower is the rate of dissociation.
- ✓ Higher the temperature higher is the rate of dissociation.
- ✓ The curves give good bi-exponential fit but fails to give single exponential fit at low density.
- ✓ At highest density the curves give good single as well biexponential fit.
- ✓ The fit parameters are presented in Table 4.1.

Figure $N(t)/N(0)$ versus time for the simulations with bath densities 20, 324, and 750 kg/m^3 and for temperature 1000, 1500, and 2000 K at each bath density

Table Fit parameters for $N(t)/N(0)$ versus time plot.

Density (kg/m^3)	T (K)	t_0 (ps)	Biexponential					Exponential
			f_1	f_2	k_1 (ps^{-1})	k_2 (ps^{-1})	$k(t_0)$ (ps^{-1})	k_{exp} (ps^{-1})
20	1000	0.70	0.450	0.550	1.500	0.270	0.823	0.420
	1500	0.60	0.550	0.450	3.100	0.400	1.885	0.906
	2000	0.55	0.600	0.400	4.100	1.200	2.940	1.700
324	1000	0.89	0.010	0.990	1.500	0.100	0.114	0.098
	1500	0.60	0.330	0.670	0.650	0.120	0.294	0.162
	2000	0.57	0.120	0.880	1.700	0.221	0.398	0.252
750	1000	4.50	0.700	0.300	0.030	0.011	0.024	0.023
	1500	1.60	0.800	0.200	0.046	0.001	0.037	0.033
	2000	1.40	0.850	0.150	0.056	0.006	0.048	0.044

Arrhenius parameters

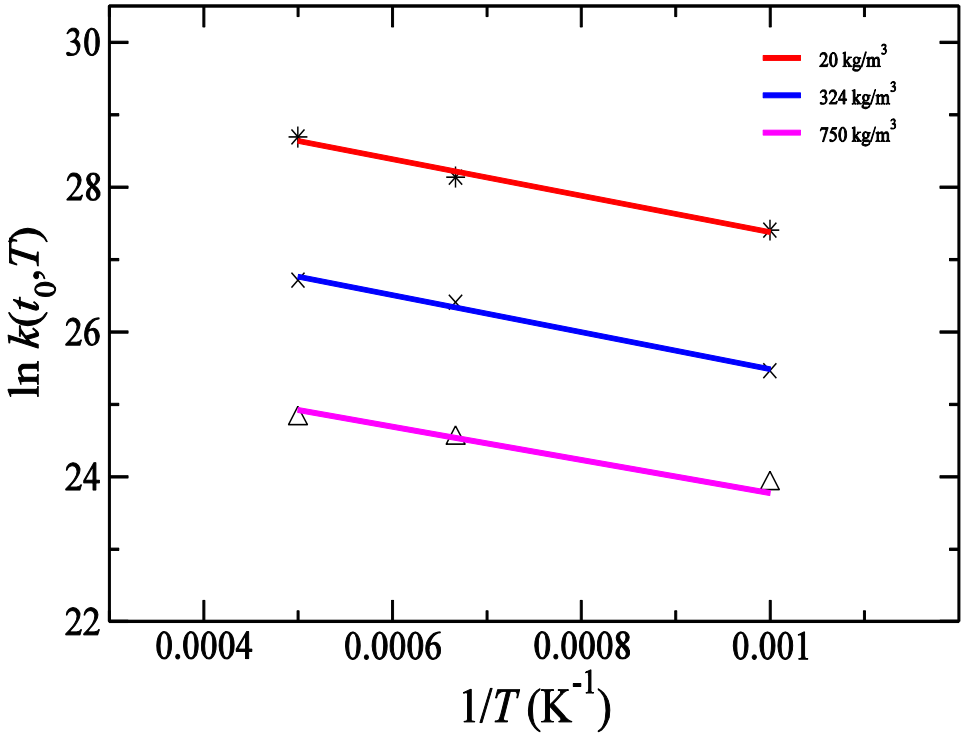

Figure ln $k(t_0,T)$ versus $1/T$ for simulations at three bath densities

Table 4.2. Arrhenius parameters for the bath densities of 20, 324, and 750 kg/m^3.

Density (kg/m^3)	Frequency factor (s^{-1})	Activation energy (E_a) (kcal/mol)
20	9.57×10^{-12}	5.04
324	1.49×10^{-12}	5.10
750	0.210×10^{-12}	4.60

- ✓ At $t = t_0$, the dynamics is RRKM in nature and the microcanonical rate constants $k(t_0,E)$ can be identical with the canonical one $k(t_0,T)$
- ✓ The E_a value is almost same for all bath density
- ✓ Pre exponential value decreases with the increase in bath density.

Comparison to Gas Phase

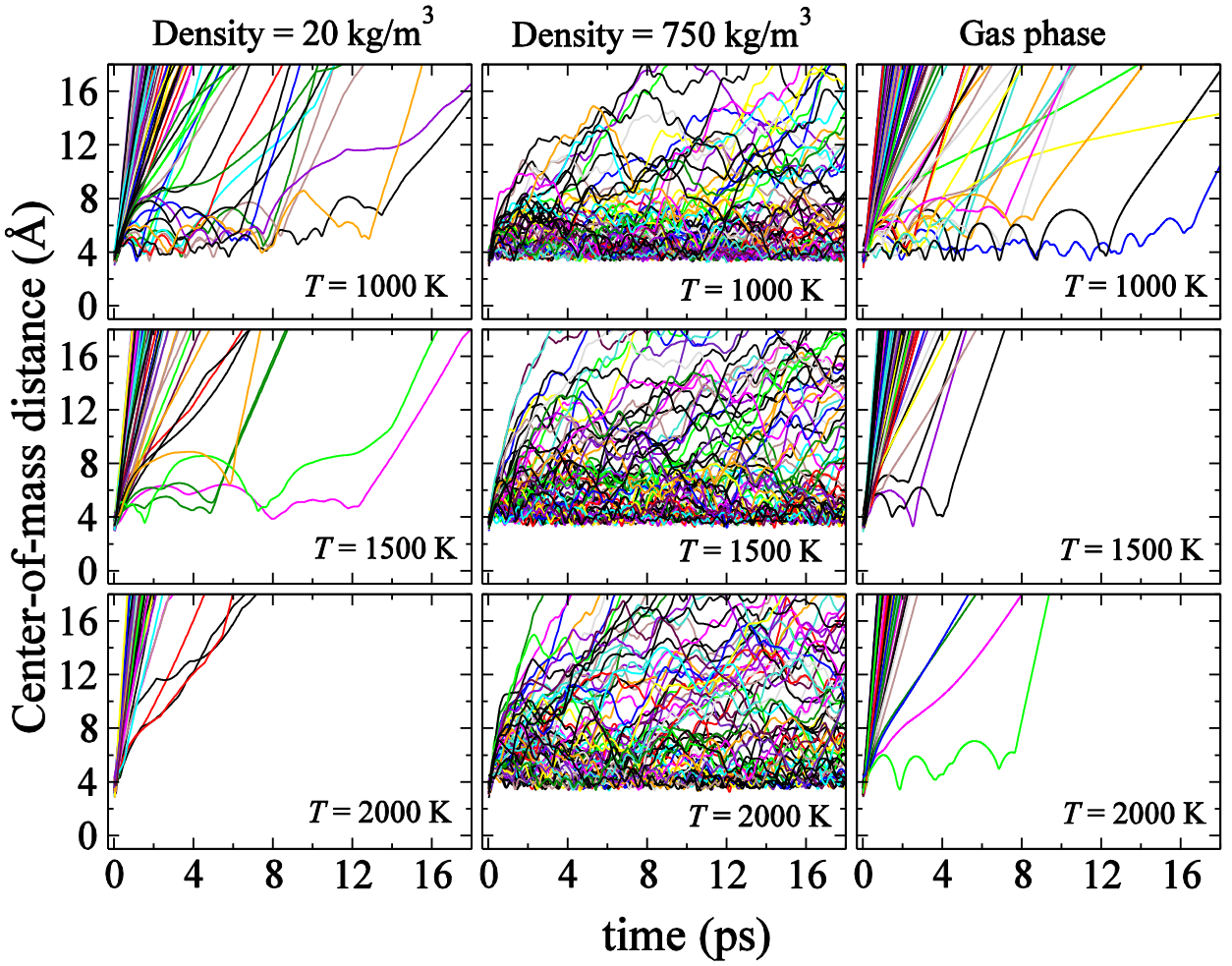

- ✓ The dissociation tendency at gas phase is very high
- ✓ The tendency is almost same for 20 kg/m^3.
- ✓ The dissociation tendency is very low at 750 kg/ m^3.

Figure Centre-of-mass distance of Bz and HFB versus time for the simulations done at N_2 bath density of 20, 750 kg/m^3, and gas phase simulation with temperature 1000, 1500, and 2000 K at each case.

H. Mahanta, D. Baishya, **S.S. Ahamed**, A.K. Paul, J. Phys. Chem. A. **123,** 2517 (2019).

➢ Energy Transfer Phenomena

Average Energy Versus Time

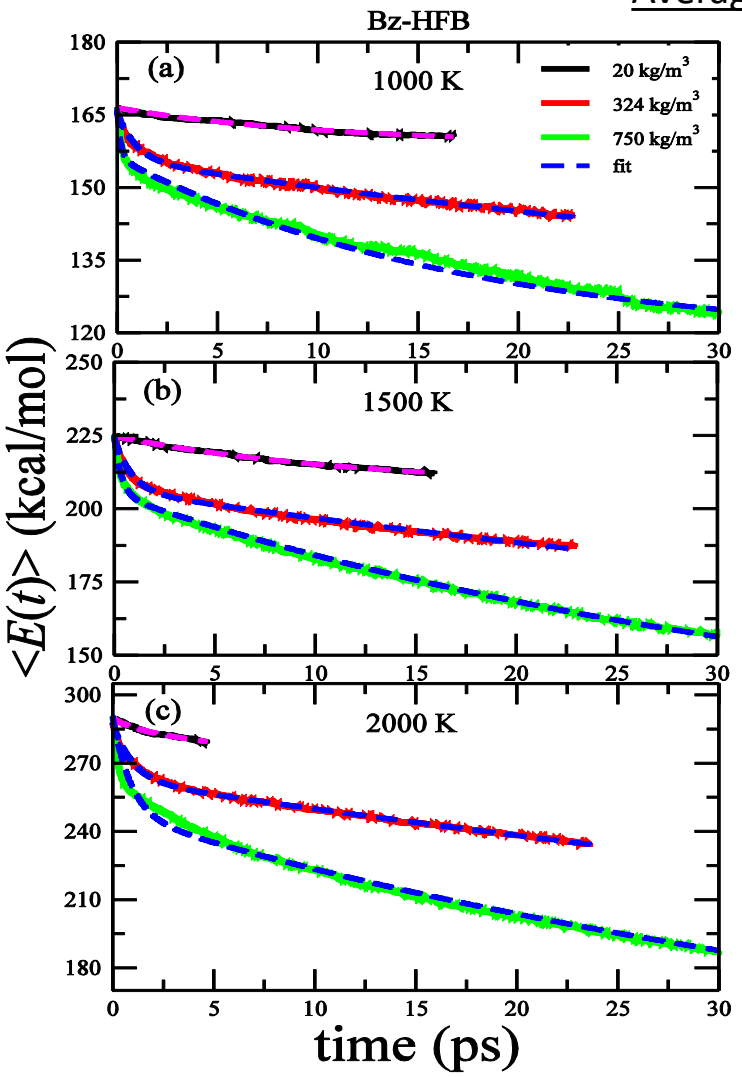

Figure plot of average solute energy versus time.

- ✓ The average energy of the complex decreases with respect to time.
- ✓ From the, it is observed that the rate of change of energy is higher for higher density.
- ✓ The lifetime of the complex is different at different temperature and bath density.
- ✓ The fitting is done using Eq. (4.6) and the parameters are given in Table 4.3.

60

Table 4.3. Parameters for fits to <*E*(t)> for different simulation condition using Eq. 4.4.

Temperature (K)	Density (kg/m^3)	Fit parameters				
		$\tilde{f}_1$	$\tilde{f}_2$	$\tilde{k}_1$ (ps^{-1})	$\tilde{k}_2$ (ps^{-1})	E_∞ (kcal/mol)
1000	20	0.107	0.893	0.1247	0.0019	117.2
	324	0.205	0.795	1.0629	0.0163	
	750	0.210	0.790	5.4270	0.0575	
1500	20	0.129	0.871	0.0951	0.0011	117.5
	324	0.170	0.830	1.1545	0.0110	
	750	0.189	0.811	2.7509	0.0271	
2000	20	0.070	0.930	0.2811	0.0021	117.8
	324	0.147	0.853	1.0284	0.0092	
	750	0.247	0.753	1.1094	0.0207	

61

Gateway Mode for Energy Transfer

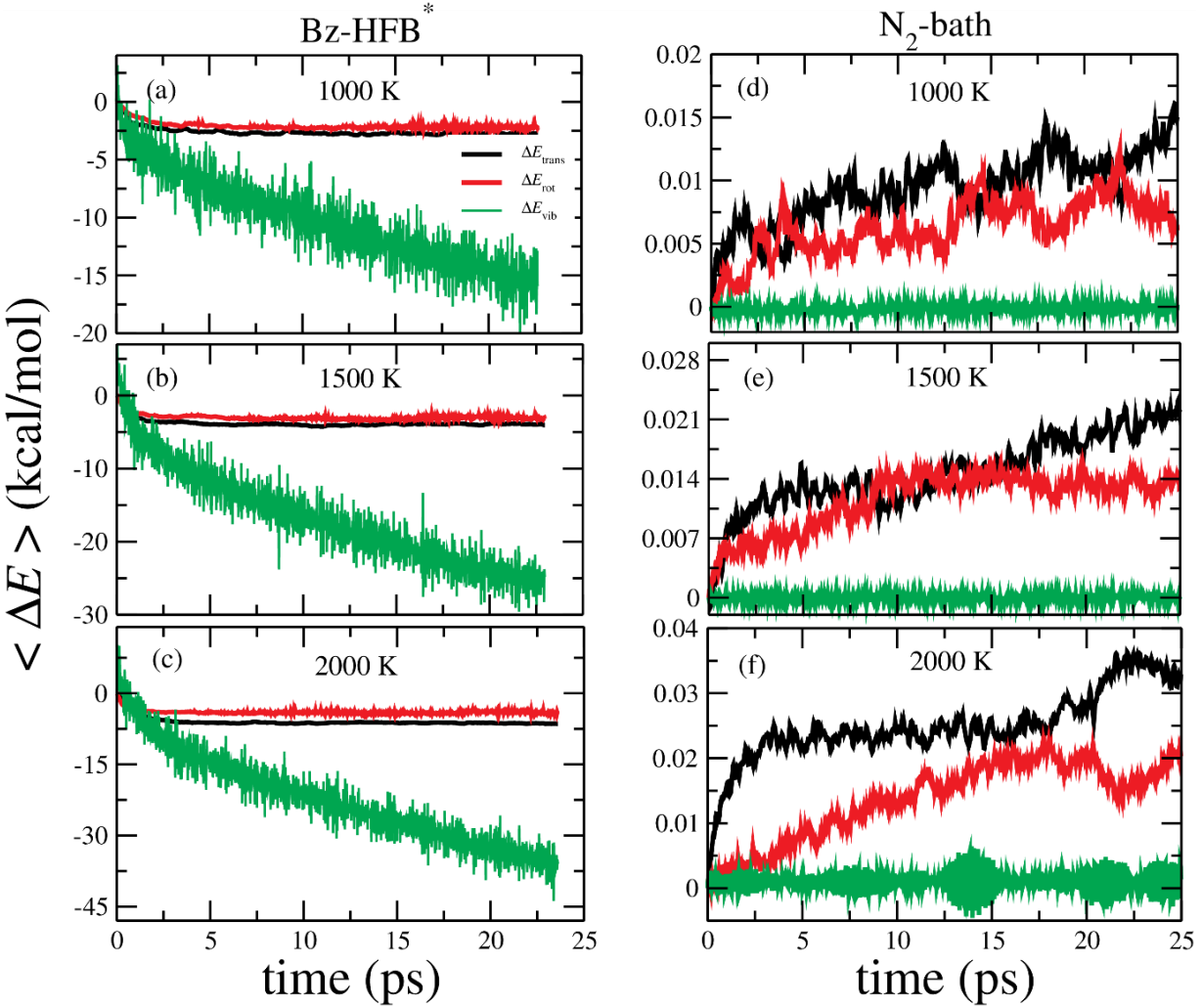

- The average center-of-mass translational, rotational and vibrational energies of Bz-HFB and bath are monitored throughout the dynamics.
- Vibrational mode of Bz-HFB is responsible for the energy transfer process.
- For the bath it is translational and rotational mode.
- The dynamics is non-statistical in nature.

Figure The change of average center-of-mass translational, rotational and vibrational energies of the Bz-HFB (a, b, and c) and the bath (d, e, and f) with respect to time.

62

Density	Bz-HFB Excitation Temperature	$k(\Delta E)^a$ ps^{-1}	$k(t_0)^a$ ps^{-1}
Gas Phase	1000 K	--	1.09
	1500 K	--	2.09
	2000 K	--	2.94
20 kg/m^3	1000 K	0.015	0.82
	1500 K	0.013	1.88
	2000 K	0.022	2.94
750 kg/m^3	1000 K	1.18	0.024
	1500 K	0.54	0.037
	2000 K	0.29	0.048

Energy transfer efficiency

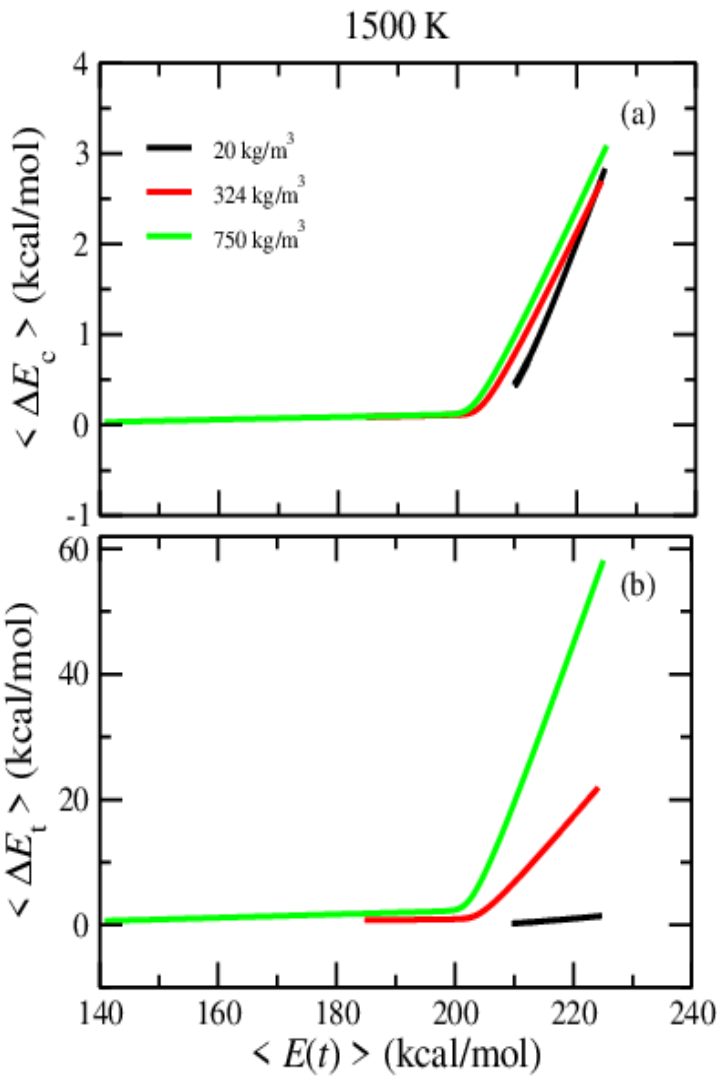

Figure Average energy transfer per collision (a) and per unit time (b) versus average total energy of Bz-HFB

- The average energy transfer per collision or per unit time is presented for initial Bz-HFB temperature of 1500 K.
- The $<\Delta E_c>$ value is very large and similar at the initial time for all three bath densities.
- $<\Delta E_c>$ become very low at longer time i.e., at lower energy of Bz-HFB.
- The collisional frequencies of N_2 + Bz-HFB system at the temperature of 1500 K and for the bath densities of 20, 324, and 750 kg/m^3 are 0.50 × 10^{12}, 8.13 × 10^{12}, and 18.8 × 10^{12} s^{-1}, respectively.

Application

- Association followed by Ensuing Dissociation in Condensed Phase

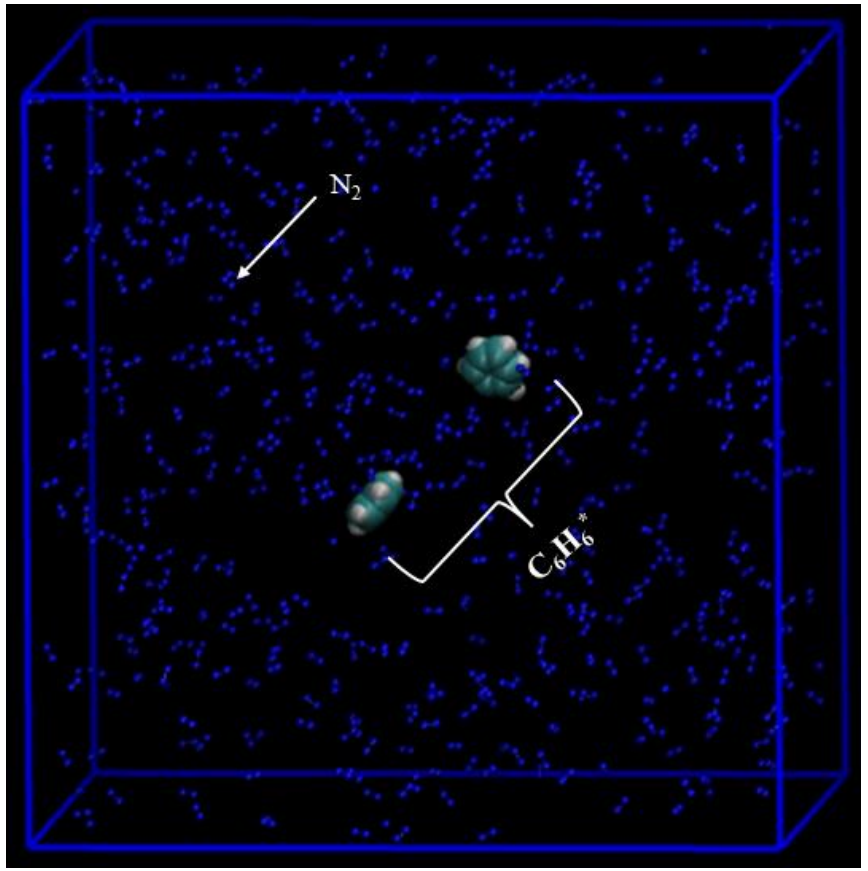

Results

$$k_{asso}(T) = \int_0^{\infty} k(E_{rel}) P(E_{rel}) dE_{rel}$$

$$k(E_{rel}) = v(E_{rel})\, \sigma(E_{rel})$$

$$\sigma(E_{rel}) = \int P_r(b).\, 2\pi b.\, db$$

$$k_{asso}(T) = \sigma(\bar{E}_{rel}) v(\bar{E}_{rel})$$

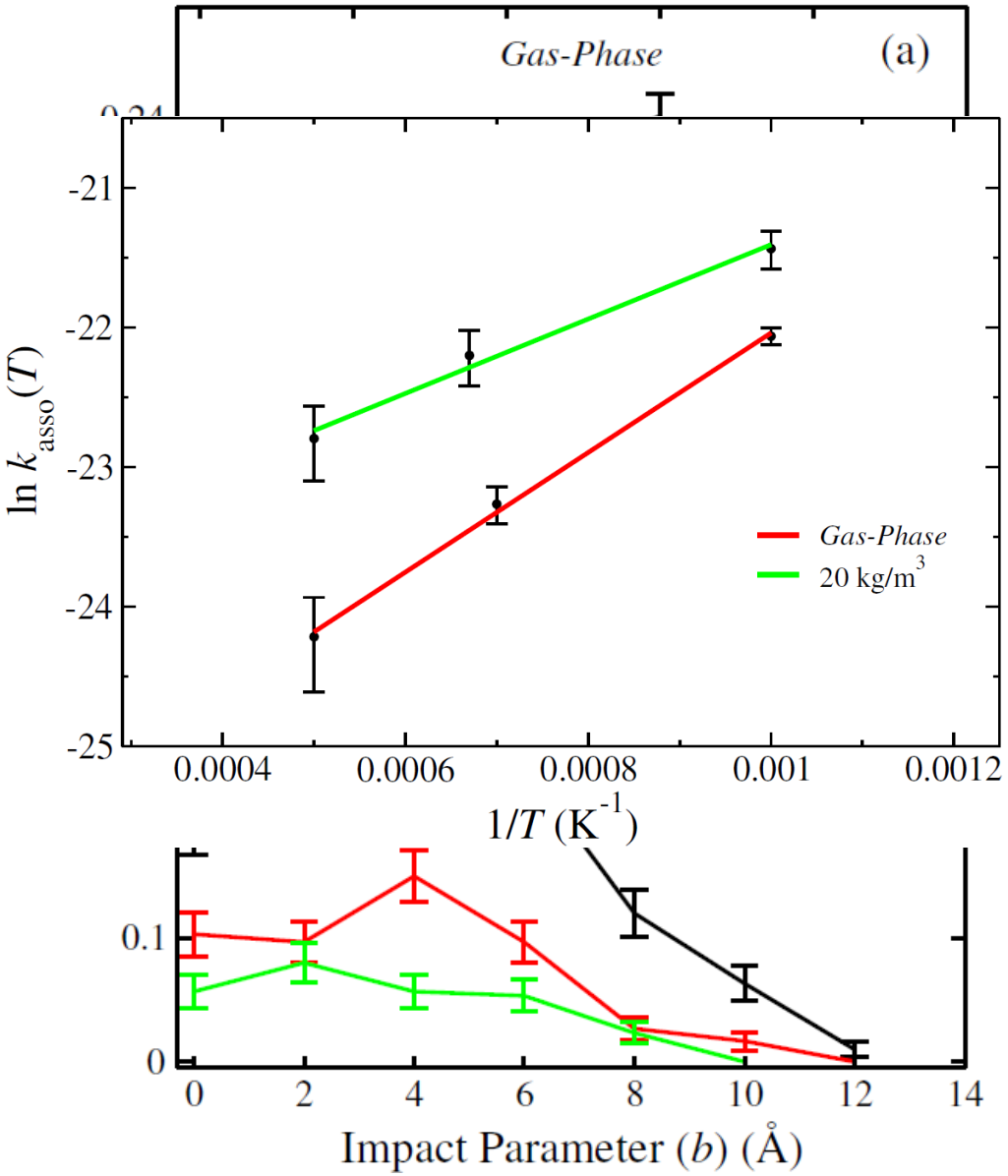

CIET

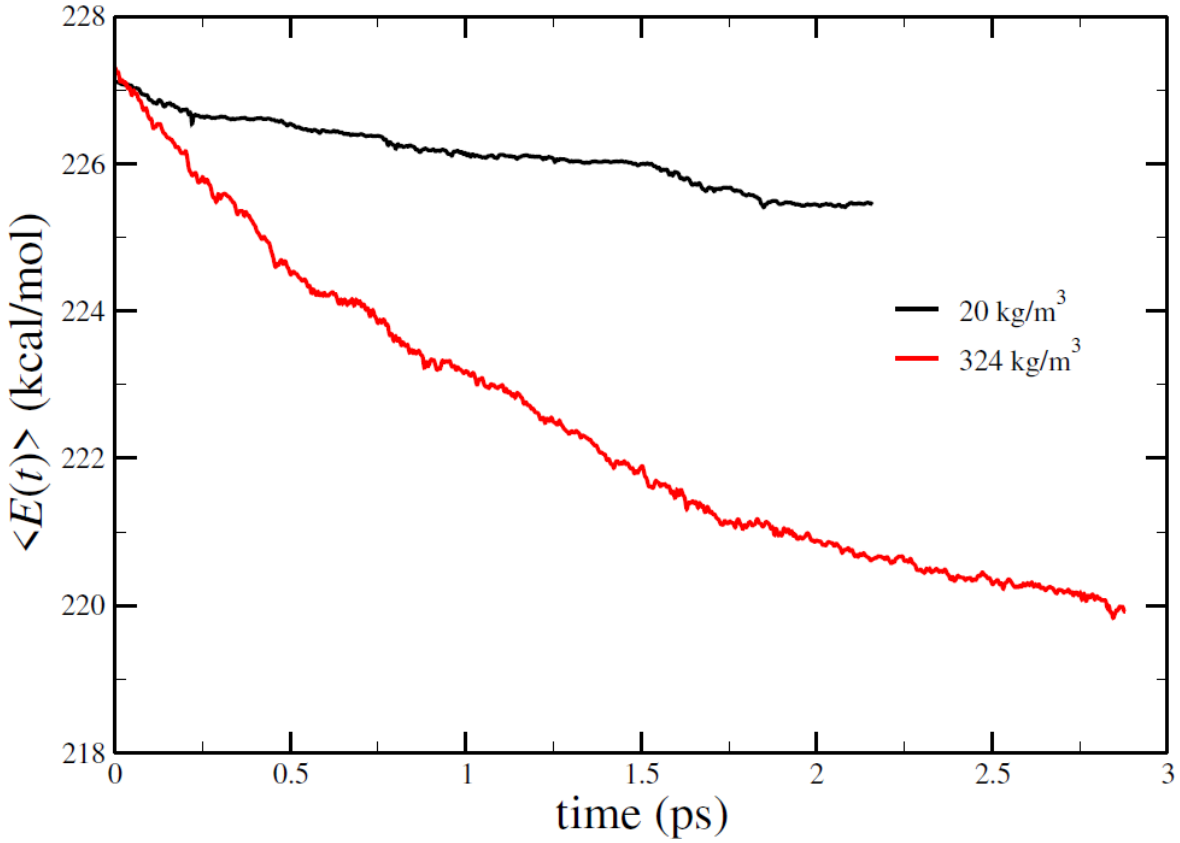

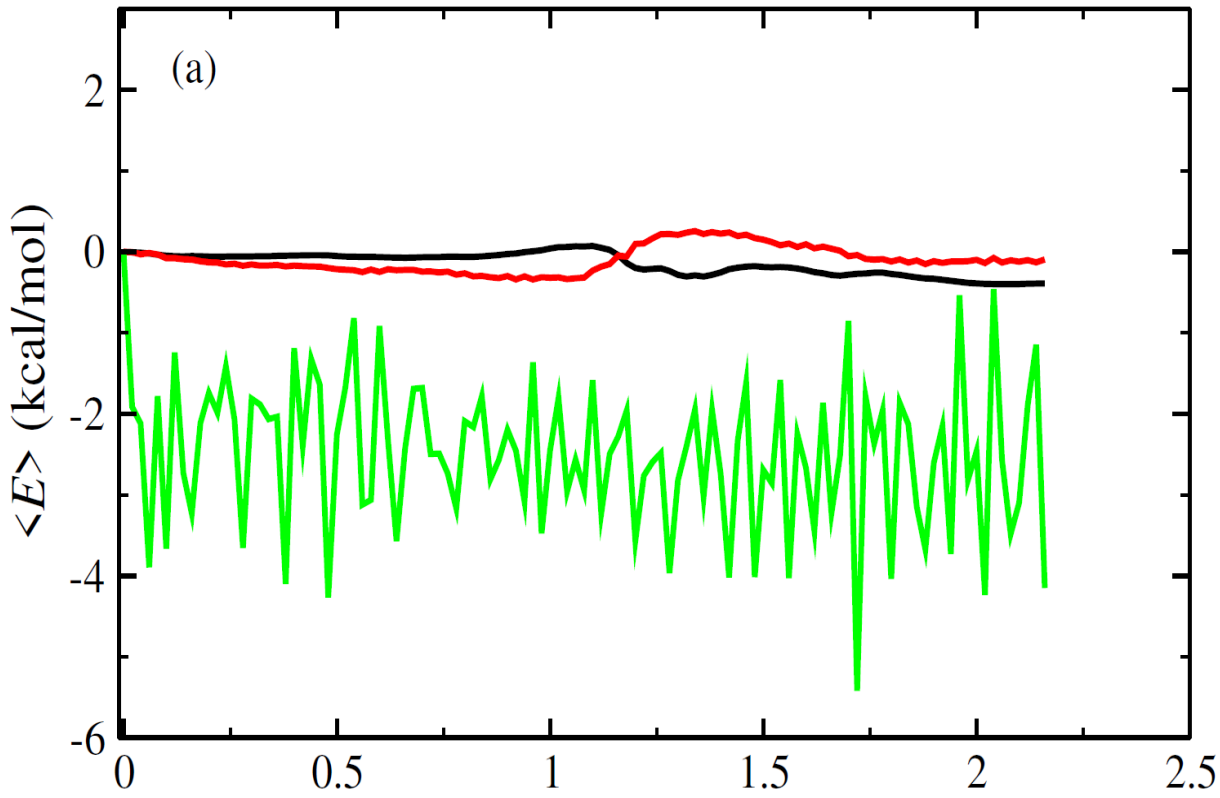

S. S. Ahamed, et al. *PCCP* 2022 (submitted)

Ensuing Dissociation Rate Constants

Temperature (K)	Impact Parameter (b)	Rate constants (ps^{-1})	
		Vacuum	Condensed Phase
1000	0	0.350	0.380
	2	0.390	0.350
	4	0.640	0.430
	6	1.65	0.475
1500	0	0.360	0.340
	2	0.460	0.310
	4	0.560	0.430
	6	3.00	0.730
2000	0	0.400	0.380
	2	0.390	0.550
	4	0.690	0.620
	6	---	0.770

CIET

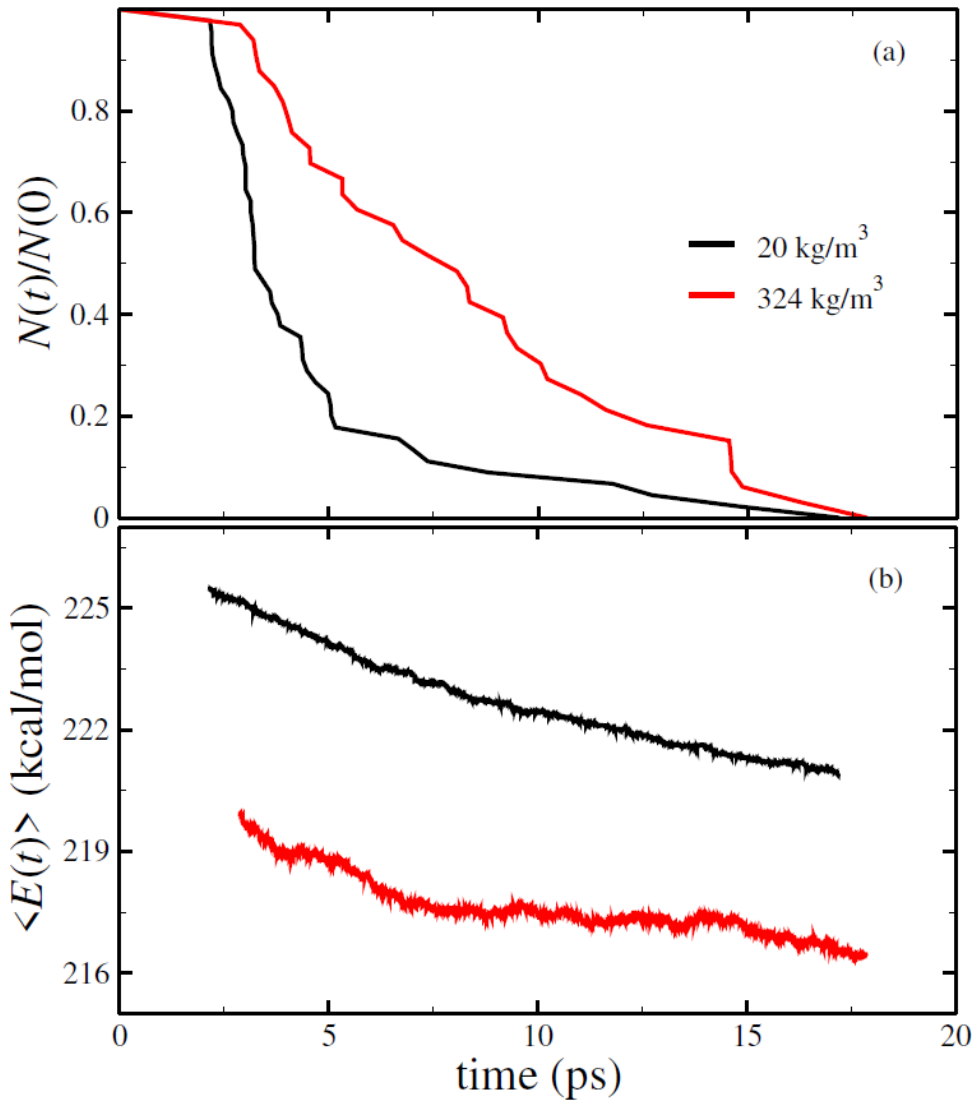

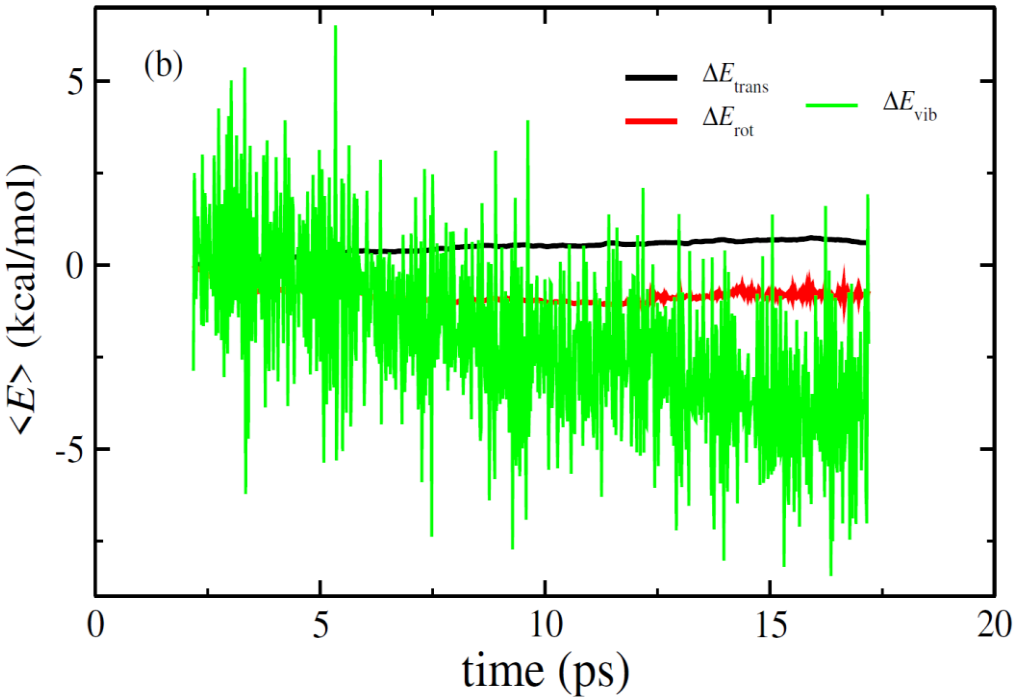

S. S. Ahamed, et al. *PCCP* 2022 (submitted)

Conclusions

The role of the surrounding molecules is crucial and needed to be considered explicitly for the reactions which are environmentally relevant

For the association reaction bath enhances the association process and delay the dissociation process. Hence longer lived complexes can be formed

Vibrational modes of the hot molecules play major role in the CIET thus, association does not disturbed.

Low frequency modes are also responsible for the energy transfer

When there is the possibility of energy transfer and dissociation processes to happen together, the energy transfer process dominates.

Application on On-the-fly Dynamics

Gas phase Ozonolysis reaction of Catechol

$$\frac{\partial q_i}{\partial t} = \frac{\partial H}{\partial p_i}; \frac{\partial p_i}{\partial t} = -\frac{\partial H}{\partial q_i}$$

$$H = T + V$$

$$T = \sum_{i=1}^{N} (P_{x_i}^2 + P_{y_i}^2 + P_{z_i}^2) / 2m_i$$

Potential Energy Calculated on-the-fly from a software

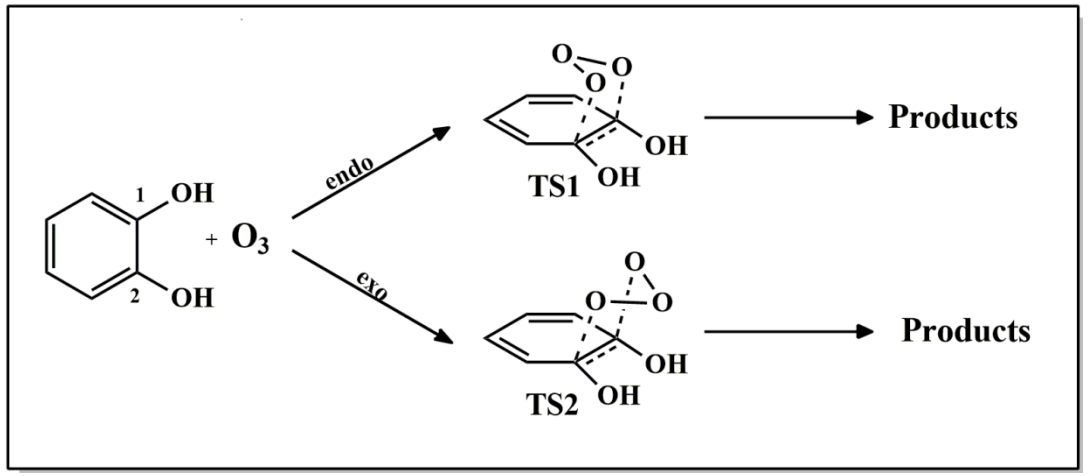

Fig1: Reaction Scheme for ozonolysis of catechol molecule.

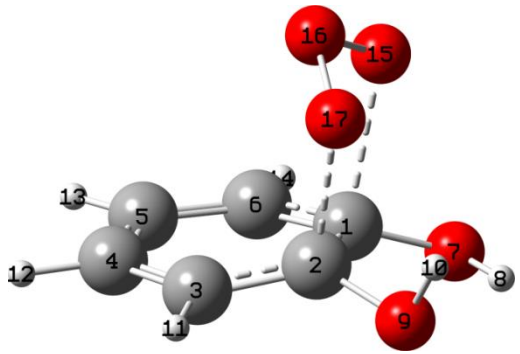

TS1 (Endo)

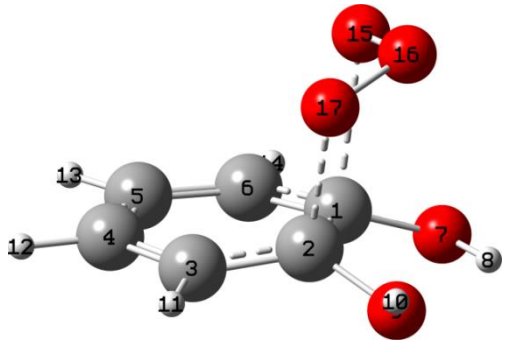

TS2 (Exo)

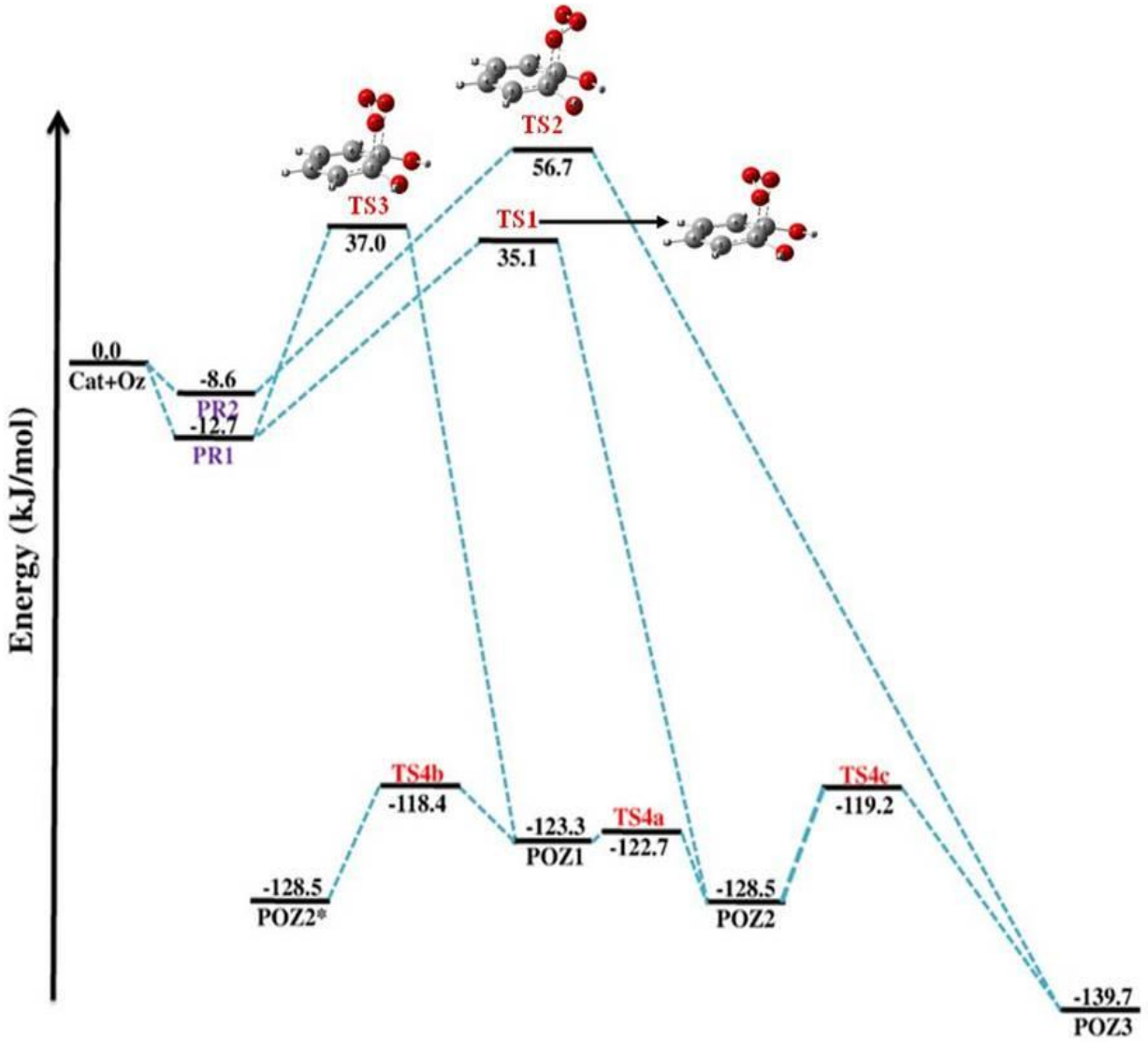

Fig2: PES of formation of primary ozonides (POZ) by1,3-cycloaddition of ozone on catechol.

Ref: Deb D. K. and Sarkar B., *Phys.Chem.Chem.Phys*. **2019**, 21, 14589

Table 1: Comparison of energies from different methods.

Methods	POZ structure	Energies in eV	Energy difference in kJ/mol
B3LYP/6-311+G(2df,2p)	Exo	-16554.48816	11.5521896864
	Endo	-16554.36843	
AM1	Exo	-2446.80982	5.6953938512
	Endo	-2446.75079	
RM1	Exo	-2413.22166	7.303766128
	Endo	-2413.14596	
MNDO	Exo	-2457.45062	5.0721134128
	Endo	-2457.39805	
PM3	Exo	-2265.97227	1.6488951536
	Endo	-2265.98936	
PM6	Exo	-2267.53846	7.0857144576
	Endo	-2267.46502	
PM7	Exo	-2288.58571	12.05584036
	Endo	-2288.46076	

- **The different geometries of reactants, transition states, and the primary ozonides (POZ) are optimized through DFT based B3LYP method with 6-311+G(2df,2p) split valence basis set using Gaussian09 software.**
- **The exo and endo POZ's are reoptimized using a semi-empirical computer program, Mopac with six different methods and the energy difference results were compared with those obtained from the B3LYP calculation.**
- **PM7 was found to be the best method.**

Simulation methodology:

- **The simulations were carried out using the Venus molecular dynamics software package interfaced with Mopac 2012.**
- **The initiation was done at the catechol-ozone transition state for the endo pathway.**
- **The energy sampling was done using the Boltzmann distribution for 400K and 500K temperatures.**
- **The trajectories were integrated using a sixth order symplectic integrator, up to 100 ps at each temperature and were terminated after 10,00,000 steps.**
- **The time was divided into discrete time steps of 0.1fs.**
- **Total energy was conserved.**
- **The trajectories were analyzed using Visual Molecular Dynamics (VMD) software.**

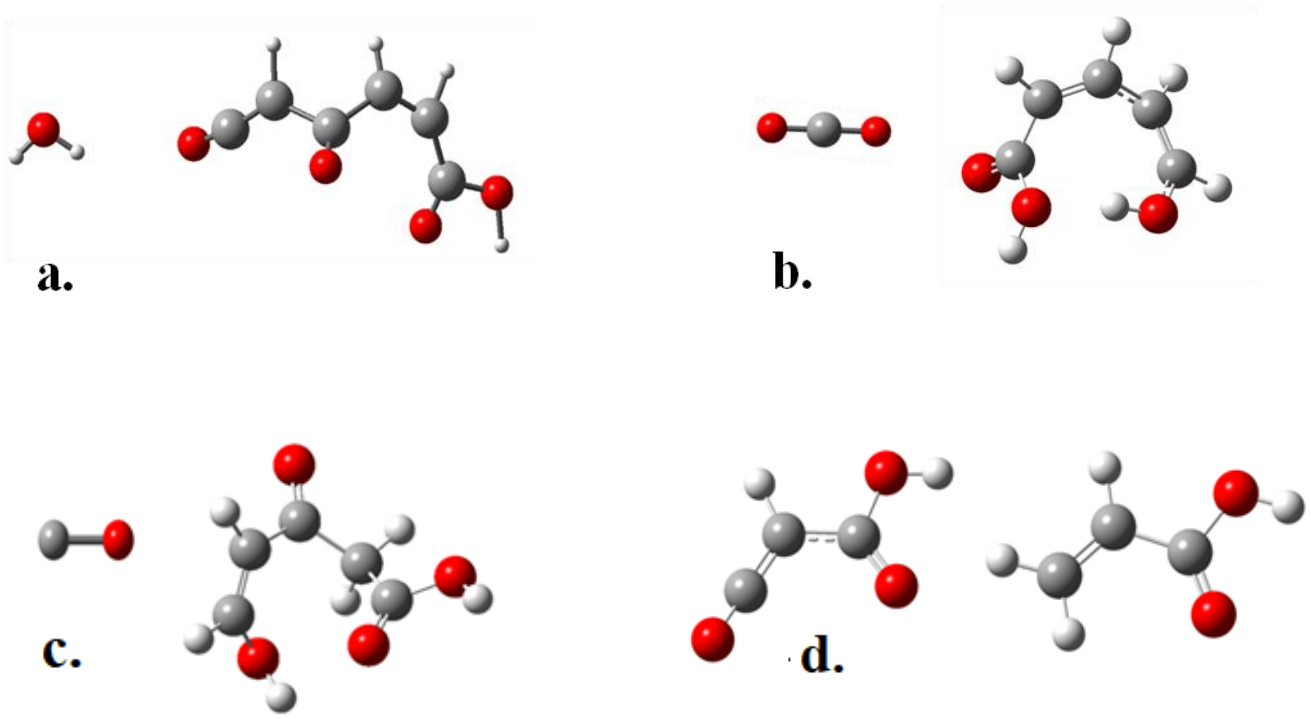

Fig.3. The four major channels observed during the ozonolysis of catechol (a) H_2O (b) CO_2 (c) CO (d) SCA.

Table 2: Total energy of the various channels.

Channels	Total Energy(kcal/mol)
CO_2	-187.6502914
H_2O	-177.4294248
CO	-157.8712243
SCA	-154.8823989
O_2	-52.92473657
$CO_2 + H_2O$	-183.8049162
$CO_2 + H_2O + CO$	-77.04743755
$CO + H_2O$	-167.2612689
$O_2 + H_2O$	-22.66248753

Table 3: Percentage of reactive, bond breaking and non-reactive channels in O_3+ Catechol reaction at 400 and 500K temperatures for TS1.

Temp.	Reactive	Bond breaking	Non reactive	Total
400K	29	57.75	13.25	100
500K	37.5	57.5	5	100

Table 4: Percentage of fragments formed at 400 and 500 K temperatures for TS1.

Temp.	CO	CO_2	Acidic	H_2O	O_2	Total
400K	27.58621	15.51724138	23.2758621	20.68966	12.93103	100
500K	30	14	25.3333333	23.33333	7.333333	100

Table 5: The energies of the four major channels alongwith the probability at 400 and 500 K.

Channel	Energy(kcal/mol)	Probability	
		400K	500K
CO_2	-187.65	13.83	15
H_2O	-177.43	36.17	28.5
CO	-157.87	29.79	33
SCA	-154.88	15.96	19

Fig.4. Bar diagram showing the variance of probability for 400K and 500K temperatures for the endo TS.

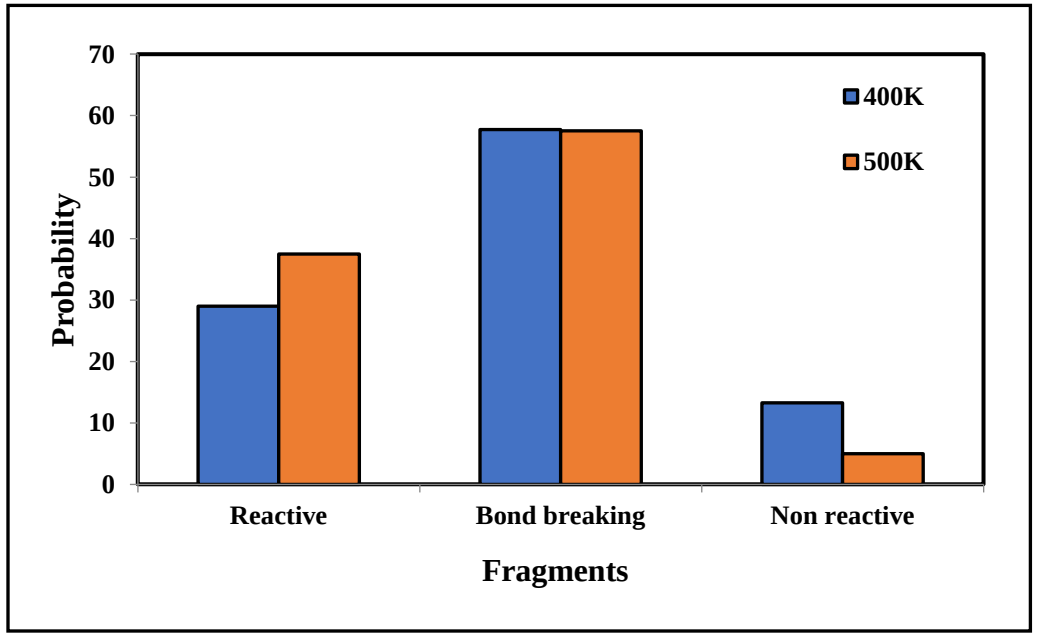

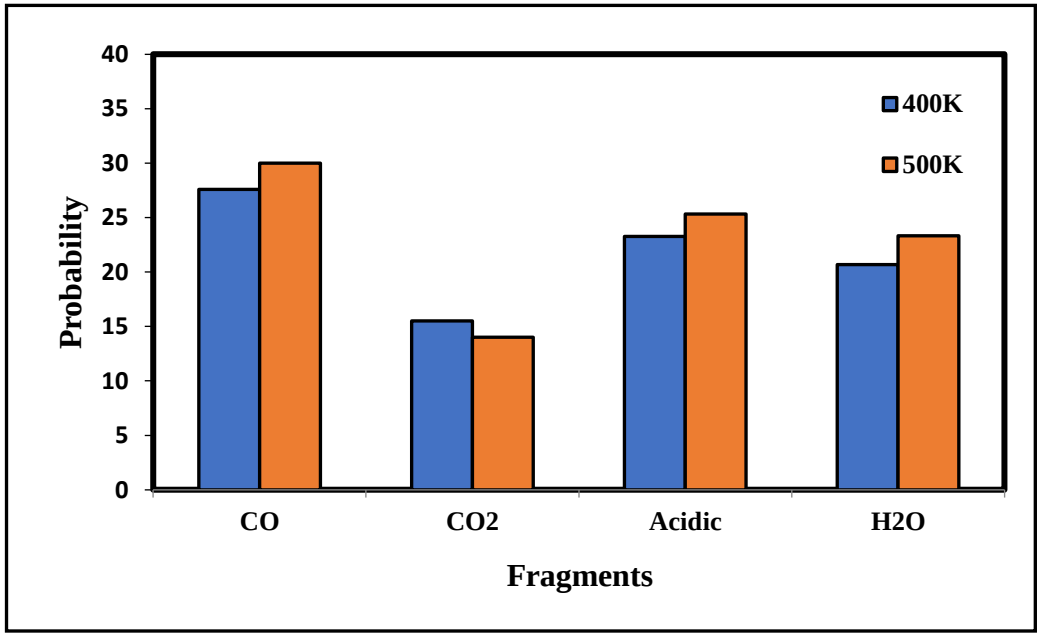

The relative number of undissociated trajectories

$$P(t) = \frac{N(t)}{N(0)} = f_1 * \exp(-k_1 t) + f_2 * \exp(-k_2\, t^{\beta(T)})$$

where N(0) is the number of trajectories at t=0
N(t) is the number of trajectories at time t.
$\beta_K(T)$ is the stretching exponent

Table 6: The rate constants and $\beta_K(T)$ for the endo TS at 400 and 500K temperatures.

Channels(400K)	k (ps^{-1})	$\beta_K(T)$	Channels(500K)	k (ps^{-1})	$\beta_K(T)$
Total reactive	$3.239*10^{-2}$	1.6	Total reactive	$3.572*10^{-2}$	1.9
CO_2	$5.148*10^{-4}$		CO_2	$2.806*10^{-4}$	
H_2O	$5.778*10^{-4}$		H_2O	$11.87*10^{-4}$	
CO	$1.406*10^{-4}$		CO	$1.426*10^{-4}$	
SCA	$1.08*10^{-4}$		SCA	$9.134*10^{-4}$	

Conclusion:

- The chemical dynamics simulations for the post transition state dynamics were performed at 400 and 500K temperatures.
- The trajectories were studied for the various channels of the reaction.
- CO channel was found to be the most probable of all the channels observed.
- With increase in temperature from 400 to 500 K the percentage of bond breaking and reactive channels has been seen to increase.
- The N_t/N_0 vs. time plots show compressed exponential behaviour, with initial slow decay, and faster decay towards the end.

Another Application

Effect of Solvent Interactions on Nonadiabatic Processes

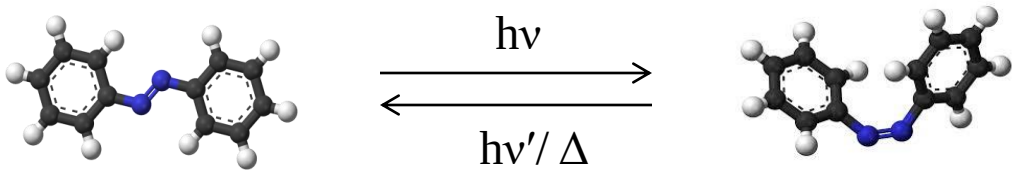

"in the absence of nonadiabatic processes life on earth as we know it would not exist."

---- **David R. Yarkony**

Introduction

❑ What is adiabatic and non adiabatic process

- In an adiabatic process an electron does not make transitions from one electronic state to others by nuclear motion.
- But in a non adiabatic process an electron can make transitions from one electronic state to others .
- The nuclear configurations of a molecule for which the electronic energy of different electronic states has exactly the same value, then the different Potential energy surface (PES) cross each-other. These processes, where coupling between different electronic states occur are called nonadiabatic processes.
- The non-adiabatic effects are due to avoided crossings of adiabatic molecular states.
- The crossing point of two adiabatic PES of the same spin multiplicity is called the conical intersection (CoIn).

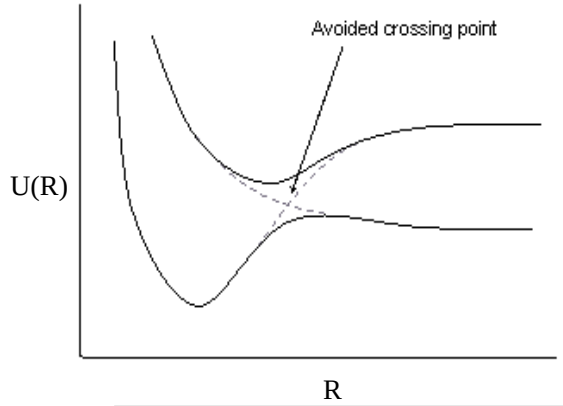

Fig. 1: Avoided crossing point

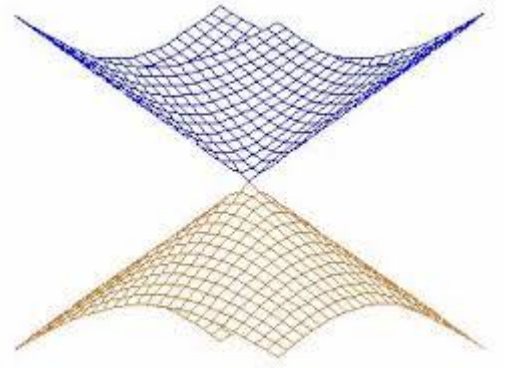

Fig.Conical intersection (CoIn) between two adiabatic PES

Fig. 1: Hund, F. *Z. Physik,* **1927,** *40*, 742.

Fig. 2: Martinez, T.J. *Nature,* **2010,** *467*, 412-413.

❑ Why Non adiabatic processes are important ?

- **Nonadiabatic phenomena are relevant in many photophysical and photochemical processes like photoisomerization, charge transfer, radiation less transitions, electronic energy transfer, quenching, etc.**
- **It includes some fundamental biochemical phenomena such as visual perception, photosynthesis, bioluminescence, DNA photodamage and repair, or vitamin D synthesis.**
- **Without consideration of non adiabatic effects it is not possible to get the correct dynamics of photochemical reactions.**

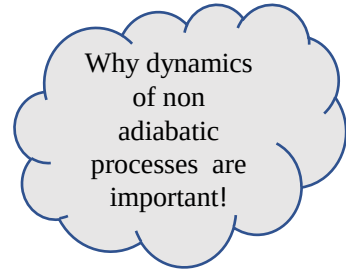

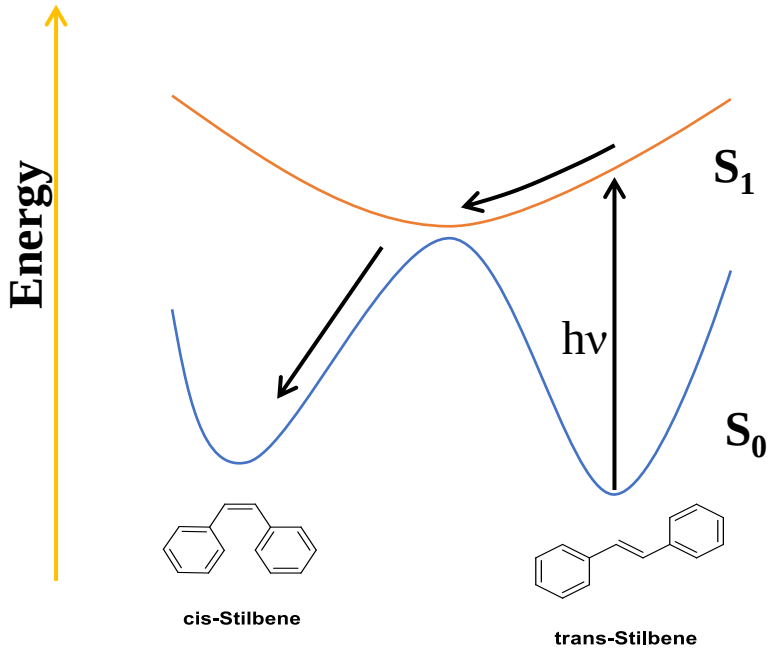

Fig. 3: A schematic diagram of potential energy surfaces for photoisomerization of Stilbene molecule.

❑ About Non - Adiabatic Coupling term

- **The Non - Adiabatic Coupling terms (NACTs) which is the outcome of the Born - Oppenheimer (BO) treatment play an important role in non adiabatic processes.**
- **According to BO treatment the the nuclear Schrodinger equation(adiabatic representation) is**

$$-\frac{\hbar^2}{2m}\begin{pmatrix}\nabla & 0 & 0\\ 0 & \nabla & 0\\ 0 & 0 & \nabla\end{pmatrix}^2\begin{pmatrix}\psi_1\\ \psi_2\\ \psi_3\end{pmatrix}+\begin{pmatrix}U_1-E & 0 & 0\\ 0 & U_2-E & 0\\ 0 & 0 & U_3-E\end{pmatrix}\begin{pmatrix}\psi_1\\ \psi_2\\ \psi_3\end{pmatrix}=0$$

The nonadiabatic coupling terms (NACTs) describe the nuclear motion when PESs are coupled.

- **The NACTs can be referred to as the off-diagonal coupling terms in kinetically coupled nuclear Schrodinger equation. It is a (n x n) matrix where n is the total electronic states. The nuclear Schrodinger equation (adiabatic representation) is**

$$-\frac{\hbar^2}{2m}\begin{pmatrix}\nabla & \tau_{12} & \tau_{13}\\ -\tau_{12} & \nabla & \tau_{23}\\ -\tau_{13} & -\tau_{12} & \nabla\end{pmatrix}^2\begin{pmatrix}\psi_1\\ \psi_2\\ \psi_3\end{pmatrix}+\begin{pmatrix}U_1-E & 0 & 0\\ 0 & U_2-E & 0\\ 0 & 0 & U_3-E\end{pmatrix}\begin{pmatrix}\psi_1\\ \psi_2\\ \psi_3\end{pmatrix}=0 \quad (2)$$

Where NAC matrix is $\tau=\begin{pmatrix}0 & \tau_{12} & \tau_{13}\\ -\tau_{12} & 0 & \tau_{23}\\ -\tau_{13} & -\tau_{12} & 0\end{pmatrix}$

- **The diabatic representation of the nuclear Schrodinger equation is**

$$\begin{pmatrix} -\frac{\hbar^2}{2m}\nabla^2 - E & 0 & 0 \\ 0 & -\frac{\hbar^2}{2m}\nabla^2 - E & 0 \\ 0 & 0 & -\frac{\hbar^2}{2m}\nabla^2 - E \end{pmatrix} \begin{pmatrix} \psi_1^d \\ \psi_2^d \\ \psi_3^d \end{pmatrix} + \begin{pmatrix} W_{11} & W_{12} & W_{13} \\ W_{21} & W_{22} & W_{23} \\ W_{31} & W_{32} & W_{33} \end{pmatrix} \begin{pmatrix} \psi_1^d \\ \psi_2^d \\ \psi_3^d \end{pmatrix} = 0 \quad (3)$$

- **The NACT(τ_{kj}) can be calculated with The Hellmann - Feynman theorem by the relation**

$$\tau_{kj}(s) = \frac{\left\langle \xi_k \left| \frac{\partial W}{\partial s} \right| \xi_j \right\rangle}{E_k - E_j} \quad (4)$$

Where W is diabatic potential energy matrix; E and ξ are the eigenvalue and eigenvector of W.

- **When the electronic states are degenerate i.e. $E_k = E_j$ then the NACT terms become singular.**
- **When NACTs are non zero, the nonadiabatic coupling terms cannot be neglected and they play an important role in non adiabatic processes. BO approximate equation fails due to the presence of the "non - adiabatic coupling" terms.**

❑ Methods used for the molecular dynamic simulation on non adiabatic processes:

- ❖ **Non-adiabatic effects in molecular dynamics can be studied with the help of classical, semiclassical, and quantum mechanical approaches.**
- ➢ **“Surface-hopping” method with its many variants can be used to study Non-adiabatic effects in molecular dynamics. The surface hopping method can be applied to a variety of situations which involve very localized regions of electronic coupling.**
- ➢ **“Fewest switches” method can also be used to show Non-adiabatic effects in molecular dynamics. With this method it can be shown that the transitions can occur anywhere, not just at localized avoided crossings.**

Strategy

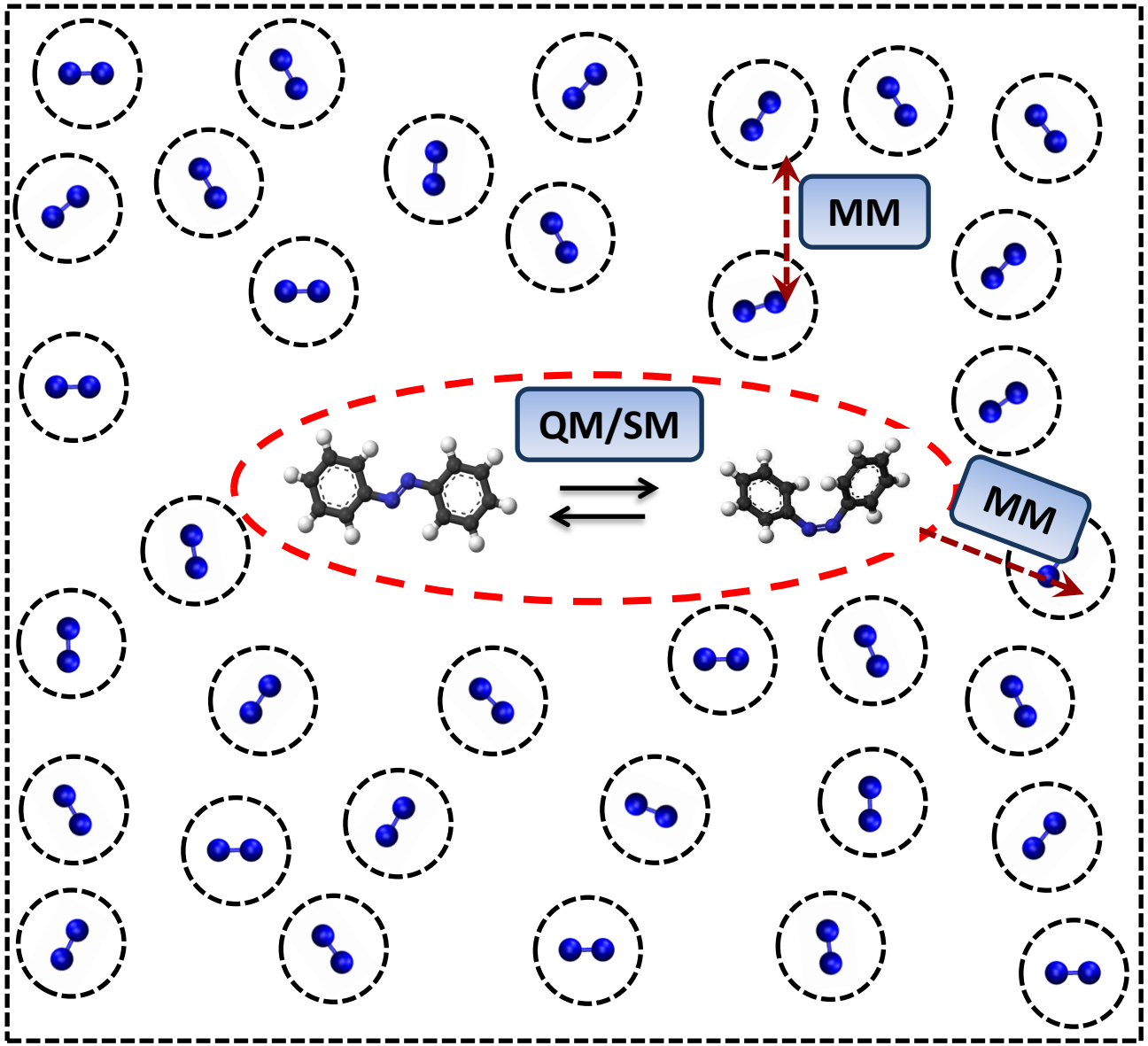

Summary

- HPC is an essential and integral part of research in chemistry
- More than 50% of the Chemist around the world use HPC for research
- Even Experimentalists some time have to depend on HPC for understanding their reactions
- Theoretical and Computational chemist only use HPC and and no other instrument. A huge benefit!!

HPC that we use

•Master Node: QTY- 1

Item	Description
Processor	2 x Intel® Xeon® Processor BDW-EP 10C E5-2630V4 (2.2GHz, 25M , 8GT QPI)
Chipset	Intel® C612 chipset
Memory	128 GB DDR4-2133 ECC RDIMM (16 x DIMM slots)
HDD	2 x 1TB Ent. SATA HDD 7.2K RPM for OS and 4 x 6TB Ent. SAS/SATA HDD 7.2K RPM for Storage
Raid	12Gb/s per port- Gen-3 - RAID 0,1,10,5,6,50,60
NIC	Dual Gigabit Ethernet onboard with suitable cable(s).
Chassis	2U Rack Mountable chassis with sliding rail kits.
Graphics	ASPEED AST2400 BMC
Management	IPMI2.0 compliant with dedicated port. Supports kvm over LAN and Virtual Media redirection, nuvoton WPCM450 BMC
Exp Slot	3PCI-E 3.0×16,3PCI-E 3.0 ×8 slots (Slot free for future upgradability)
P. Supply	740W Redundant Power Supplies 80 PLUS, Platinum Level (94%)
OS	CentOS Enterprise Linux
Warranty	3-year Parts, 3-year labour, 3-year onsite Supports NBD On hardware Only

•Compute Node: QTY- 4

Item	Description
Processor	2 x Intel® Xeon®Processor BDW-EP 10C E5-2630V4 2.2GHz 25M 8GT QPI
Memory	128 GB DDR4-2133 ECC RDIMM (Max Up to 1 TB)
Storage Compute	1×2000 GB Enterprise SATA,SATA Support, 3×Hot-swap SAS/SATA Drive Bays for each node
Gigabit Ethernet	Intel® i350 Dual Port Gigabit Ethernet onboard with suitable cable(s).
Chasis	0.5U effective form factor (4 independent compute nodes share single 2U chasis and power supply)
Graphics	Integrated
Management	IPMI 2.0 compliant with dedicated port. supports KVM over LAN and virtual media redirection.
Ports	1 (×16) PCI-E (Low Profile) (slot free for future upgradability)
P. Supply	1600 W Redundant Power Supplies Titenium Level (96%)
OS	CentOS Enterprise Linux
Warranty	3-year Parts, 3-year labour, 3-year onsite Supports NBD On hardware Only

Acknowledgement

Ph.D. Students:

Sk. Samir Ahamed

Dr. Himashree Mahanta

Palash Jyoti Boruah

Ankita Agarwal

Basudha Deb

Manju Yadav

And Many M.Sc. Project Student:

Funding

Facilities